Dalton Transactions

An international journal of inorganic chemistry

Accepted Manuscript

This article can be cited before page numbers have been issued, to do this please use: G. Orton, J. K. Cockcroft, M. R. Ringenberg, F. Hartl and G. Hogarth, *Dalton Trans.*, 2026, DOI: 10.1039/D6DT00946H.

ROYAL SOCIETY OF CHEMISTRY

rsc.li/dalton

View Article Online
DOI: 10.1039/C5DT00946H

[FeFe]-hydrogenase biomimics incorporating redox-active ligands: Tuning the oxidation chemistry of ferrocene–dichalcogenolate-bridged centres via phosphine substitution

Georgia R. F. Orton [a,b], Jeremy K. Cockcroft [c], Mark R. Ringenberg [d], František Hartl [e]* and Graeme Hogarth [a]*

[a] Department of Chemistry, King's College London, 7 Trinity Street, London, SE1 1DB, UK
[b] School of Chemistry, University of Birmingham, Edgbaston, Birmingham B15 2TT, UK
[c] Department of Chemistry, University College London, 20 Gordon Street, London, WC1H 0AJ, UK
[d] Institut für Anorganische Chemie, Universität Stuttgart, Pfaffenwaldring 55, 70569 Stuttgart, Germany
[e] Department of Chemistry, University of Reading, Whiteknights, Reading RG6 6DX, UK

Abstract

Ferrocene–dichalcogenolate-bridged complexes, $[Fe_2(CO)_6\{\mu\text{-}E(\eta^5\text{-}C_5H_4)Fe(\eta^5\text{-}C_5H_4)E)\}]$ (E = S, Se), are [FeFe]-hydrogenase biomimics, in which the two redox-active centres lie in close proximity. Here we report the syntheses and electrochemical studies of phosphine-substituted derivatives, which allows tuning of the oxidation chemistry of the Fe_2 centre, while (effectively) leaving that of the ferrocene centre unchanged. Mono-substituted $[Fe_2(CO)_5\{\mu\text{-}Se(\eta^5\text{-}C_5H_4)Fe(\eta^5\text{-}C_5H_4)Se)\}(Ph_2P\text{-}p\text{-tolyl})]$, chelated $[Fe_2(CO)_4\{\mu\text{-}E(\eta^5\text{-}C_5H_4)Fe(\eta^5\text{-}C_5H_4)E)\}(\kappa^2\text{-}dppv)]$ and bridged $[Fe_2(CO)_4\{\mu\text{-}E(\eta^5\text{-}C_5H_4)Fe(\eta^5\text{-}C_5H_4)E)\}(\mu\text{-}dppf)]$ complexes have been prepared under carefully controlled reaction conditions, the selenium derivative giving higher yields. Crystal structures of $[Fe_2(CO)_4\{\mu\text{-}Se(\eta^5\text{-}C_5H_4)Fe(\eta^5\text{-}C_5H_4)Se)\}(\kappa^2\text{-}dppv)]$ and $[Fe_2(CO)_4\{\mu\text{-}Se(\eta^5\text{-}C_5H_4)Fe(\eta^5\text{-}C_5H_4)Se)\}(\mu\text{-}dppf)]$ have been determined, which contain three closely located iron redox centres. Cyclic voltammetry (CV) and IR spectroelectrochemistry (IR SEC) have been used to understand changes occurring upon oxidation. Upon successive replacement of carbonyl(s), the oxidation potential of the Fe_2 centre is lowered and in the dppv and dppf complexes it occurs prior to oxidation of the remote Fe(II) centre in the ferrocene–dithiolate bridge, as confirmed by IR SEC experiments. Dppf complexes contain three different iron oxidation centres, and three separate oxidation waves are identified in the CV of

View Article Online
DOI: 10.1039/b00000000H

$[Fe_2(CO)_4\{\mu\text{-Se}(\eta^5\text{-}C_5H_4)Fe(\eta^5\text{-}C_5H_4)Se\}(\mu\text{-dppf})]$. DFT calculations have been used to better understand the likely structures of the oxidised species. They suggest that oxidation of the Fe_2 centre results in a structural rearrangement to give a semi-bridging carbonyl, but no such species are observed by IR SEC, possibly due to the high rearrangement energies. IR SEC studies also suggest that for the dppf complexes, oxidation may be delocalised over several sites.

Keywords: hydrogenase; biomimetic; phosphines; redox tuning; oxidation; spectroelectrochemistry; ferrocene

1 Introduction

The H-cluster site of [FeFe]-hydrogenases contains two redox centres, viz. the Fe_2S_2 core and a pendant Fe_4S_4 cluster[1-5] and their strong electronic coupling is a key feature of the enzymatic catalytic functionality.[6-8] Over the past two decades, biomimics of [FeFe]-H_2ases have been extensively studied[9-20]; however, in the vast majority of these studies the focus has centred exclusively on the chemistry and redox properties of the Fe_2 centre and, in comparison, systems containing a second redox active site that can act as a surrogate for the Fe_4S_4 cluster, are (relatively) rare.[21-30] Another feature of [FeFe]-H_2ase biomimics is a focus on their reduction chemistry and ability to catalyse proton reduction, while in contrast their oxidation chemistry, crucial for hydrogen oxidation catalysis, has largely been neglected.[31-38] A current theme of our work in this area[39-46] is the introduction of redox-active co-ligands to prepare biomimics containing two or more oxidizable redox centres, with the aim of preparing functional H_2 oxidation catalysts.

In this context, we recently detailed studies of ferrocene–dichalcogenolate-bridged complexes, $[Fe_2(CO)_6\{\mu\text{-E}(\eta^5\text{-}C_5H_4)Fe(\eta^5\text{-}C_5H_4)E)\}]$ (E = S (**1**), Se (**2**))[47,48] using cyclic voltammetry (CV), IR spectroelectrochemistry (IR SEC) and density functional theory (DFT) calculations to probe changes occurring upon oxidation and reduction.[45,46] While the ferrocene centre is fully reversibly oxidised at relatively low potentials, oxidation of the Fe_2S_2 core is outside of the CH_2Cl_2 electrolyte potential window, preventing the generation of the doubly oxidised species envisaged to be necessary to oxidize H_2. An established way of lowering the oxidation potential of the Fe_2S_2 centre is the sequential replacement of one or more carbonyls with strongly electron-donating ligands such as phosphines or carbenes.[49] In this way, the oxidation potential of

View Article Online
DOI: 10.1039/D0DT00946H

the Fe_2S_2 sub-unit can be tuned and brought closer to that of the ferrocenyl centre, potentially allowing strong electronic coupling between the two sites. Carbonyl substitution in $[Fe_2(CO)_6(\mu$-dithiolate)] complexes containing a flexible dithiolate bridge is (usually) relatively straightforward, requiring only mild reaction conditions and giving high product yields, as exemplified by the substitution chemistry of $[Fe_2(CO)_6(\mu$-pdt)] (pdt = 1,3-propane-dithiolate).[50-60] In contrast, for those with rigid dithiolate bridges, substitution often requires more forcing conditions and can lead to low product yields. This is exemplified by $[Fe_2(CO)_6(\mu$-bdt)] (bdt = 1,2-benzene-dithiolate) and related derivatives, which are also susceptible to fragmentation of the diiron centre and consequent formation of mononuclear products.[61-67] Reasons for this behaviour are (likely) linked to the associative nature of ligand substitution at non-bridged and flexible-bridge diiron dithiolate complexes,[68-70] which requires formation of an expanded non-Fe–Fe bonded intermediate. Sluggish carbonyl substitution can be circumvented by promoting a dissociative pathway, either via addition of a decarbonylating reagent such as Me_3NO or under photolysis.[70] Herein we describe the successful syntheses of some mono and di-phosphine-substituted derivatives of **1** and **2**. Reaction conditions must be carefully chosen and controlled, and even then, yields are low, especially for derivatives of dithiolate-containing **1**, while (in general) the diselenolate-based chemistry gives higher yields. Nevertheless, this approach gives access to [FeFe]-H_2ase biomimics containing two or three redox-active metallic sites, allowing an investigation of their oxidation behaviour by CV and IR SEC, the results of which are supported by DFT studies.

2 Results and Discussion

2.1. Synthesis of $[Fe_2(CO)_5\{\mu$-Se(η^5-C_5H_4)Fe(η^5-C_5H_4)Se)}(Ph_2P-*p*-tolyl)] (3)

We initially targeted PAr_3-substituted complexes and selected Ph_2P-*p*-tolyl since the methyl group serves as a useful NMR reporter. After several unsuccessful attempts (see ESI) we prepared **3** using a low-temperature CO-dissociative route.[71,72] Thus, decarbonylation of a THF solution of **2** by Me_3NO at –25 °C in the presence of excess Ph_2P-*p*-tolyl resulted in the formation of $[Fe_2(CO)_5\{\mu$-Se(η^5-C_5H_4)Fe(η^5-C_5H_4)Se)}(Ph_2P-*p*-tolyl)] (**3**) in moderate (30–40%) yields (**Scheme 1**). No evidence was obtained for a disubstituted complex, even after refluxing an MeCN solution of **3** with an excess Ph_2P-*p*-tolyl for 12 h. The IR spectrum of **3** shows the characteristic ν(CO) band pattern with four maxima at 2037s, 1982vs, 1962br and

View Article Online
DOI: 10.1039/D0DT00946H

1920w cm^{-1}. The reaction of **1** with Ph_2P-*p*-tolyl under similar conditions resulted in trace formation of $[Fe_2(CO)_5\{\mu\text{-}S(\eta^5\text{-}C_5H_4)Fe(\eta^5\text{-}C_5H_4)S\}(Ph_2P\text{-}p\text{-tolyl})]$ (see ESI) but all attempts to obtain a pure sample were unsuccessful.

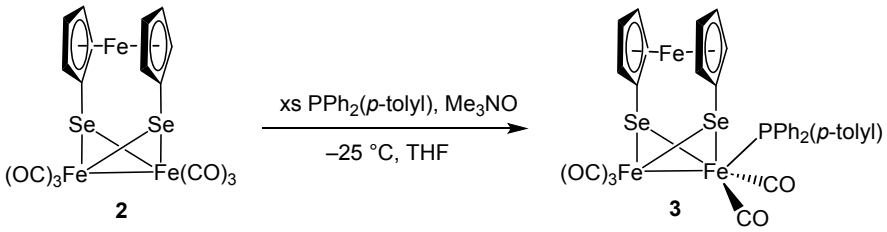

Scheme 1 Synthesis of $[Fe_2(CO)_5\{\mu\text{-}Se(\eta^5\text{-}C_5H_4)Fe(\eta^5\text{-}C_5H_4)Se\}(Ph_2P\text{-}p\text{-tolyl})]$ (**3**).

In $[Fe_2(CO)_5(PAr_3)(\mu\text{-dithiolate})]$ complexes the phosphine invariably occupies an apical site, and this is the case for **3** as revealed by NMR spectroscopy. Thus, for an apically bound phosphine, four ferrocenyl proton environments would be expected, whereas for the basal isomer all eight ferrocenyl protons are inequivalent. In the ^1H NMR spectrum of **3** (**Fig. 1**), three ferrocenyl proton environments are observed (ratio 2:2:4), thereby confirming an apical phosphine.

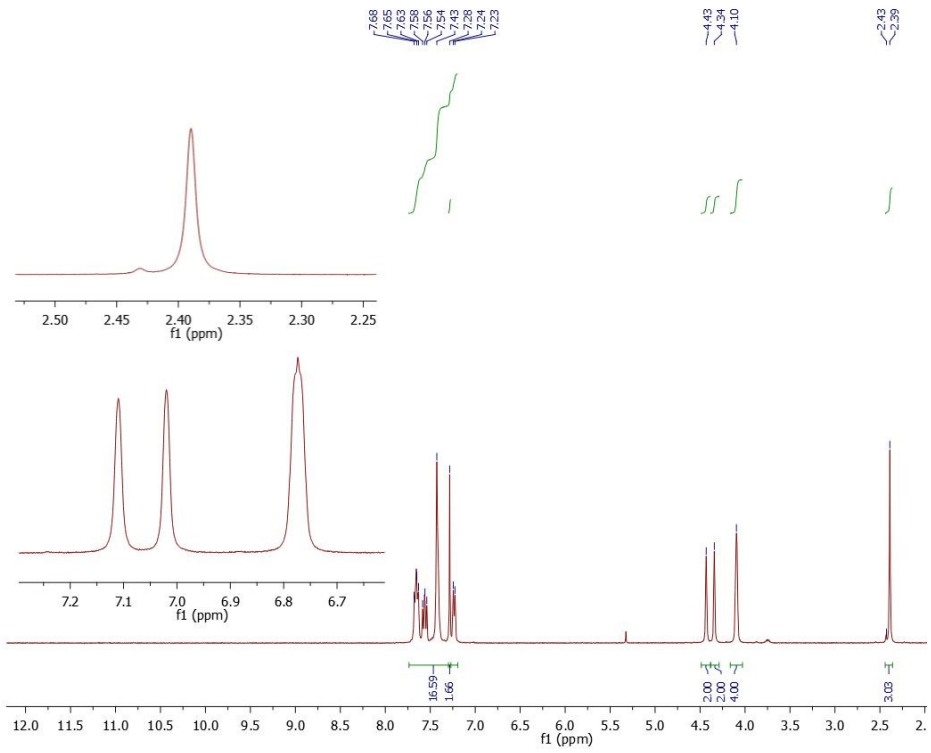

Fig. 1 ^1H NMR spectrum of **3** in $CDCl_3$ with inserts of the alkyl and ferrocenyl regions.

2.2. Synthesis of $[Fe_2(CO)_4\{\mu\text{-}E(\eta^5\text{-}C_5H_4)Fe(\eta^5\text{-}C_5H_4)E\}(\kappa^2\text{-dppv})]$ (E = S (4) and Se (5))

Asymmetry at the diiron centre has been identified as a desirable feature of [FeFe]-H_2ase biomimics[73] and both steric and electronic asymmetry can be introduced through the coordination of chelating diphosphines. *cis*-1,2-Bis(diphenylphosphino)ethene (dppv) has been widely used in [FeFe]-H_2ase biomimics as it invariably yields chelate complexes.[74-78] Dppv-substituted $[Fe_2(CO)_4\{\mu\text{-}S(\eta^5\text{-}C_5H_4)Fe(\eta^5\text{-}C_5H_4)S\}(\kappa^2\text{-dppv})]$ (**4**) and $[Fe_2(CO)_4\{\mu\text{-}Se(\eta^5\text{-}C_5H_4)Fe(\eta^5\text{-}C_5H_4)Se\}(\kappa^2\text{-dppv})]$ (**5**) were prepared upon addition of dppv to THF solutions of **1** and **2** at ca. –20 °C after the treatment with two equivalents of $Me_3NO{\cdot}2H_2O$ (**Scheme 2**). After 20 min the solution was warmed to 40 °C and stirred for ca. 1 h, when IR spectra showed consumption of **1–2**. Chelate formation is apparent from the characteristic IR pattern associated with an $[Fe_2(CO)_4(\mu\text{-dithiolate})(\kappa^2\text{-diphosphine})]$ complex [ν(CO) **4**: 2025vs, 1956s, 1914w cm^{-1}; ν(CO) **5:** 2017vs, 1949s, 1911w cm^{-1}]. The $^{31}P\{^1H\}$ NMR spectrum of **4** shows two broad singlets consistent with the axial-basal isomer, their broad nature being associated with a fluxional process (not explored due to the low yields). For **5**, the $^{31}P\{^1H\}$ NMR spectrum contains a singlet at δ 84.3 and the ^1H NMR spectrum features four cyclopentadienyl environments, both observations being consistent with the formation of a dibasal isomer. In a concentrated sample of **5**, two small peaks (ca. 2%) at 93.6 and 80.5 ppm were also observed in the $^{31}P\{^1H\}$ NMR spectrum, likely due to a small amount of the axial-basal isomer. Reasons why the change in the dichalcogenolate results in the different isomers are not obvious but may originate from the larger selenium atoms and the more diffuse lone pairs, which favours the dibasal form.

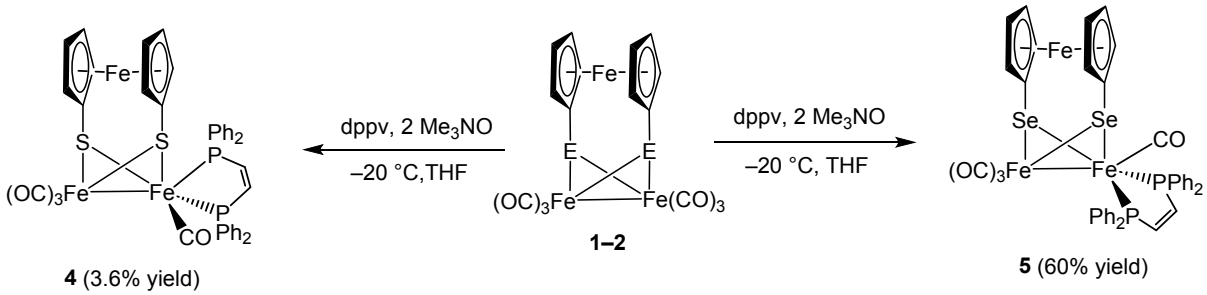

Scheme 2 Synthesis of $[Fe_2(CO)_4\{\mu\text{-}E(\eta^5\text{-}C_5H_4)Fe(\eta^5\text{-}C_5H_4)E\}(\kappa^2\text{-dppv})]$ (E = S (**4**) and Se (**5**))

View Article Online
DOI: 10.1039/D6DT00946H

Single crystals of **5** were grown by slow diffusion of hexanes into a concentrated CH_2Cl_2 solution. The structure confirms that diphosphine is dibasal, thus minimizing adverse interactions between bridgehead and diphosphine (**Fig. 2**). The Fe–Fe bond is slightly longer than that in **2** [2.5507(5) Å in **2** vs. 2.6857(7) Å in **5**].[48] The distance from the ferrocenyl Fe centre to the phosphine-substituted iron is 4.3664(7) Å, and to the distal Fe centre 4.3491 (7) Å, both being slightly shorter than those observed in **2** (4.401 (6) Å).[48]

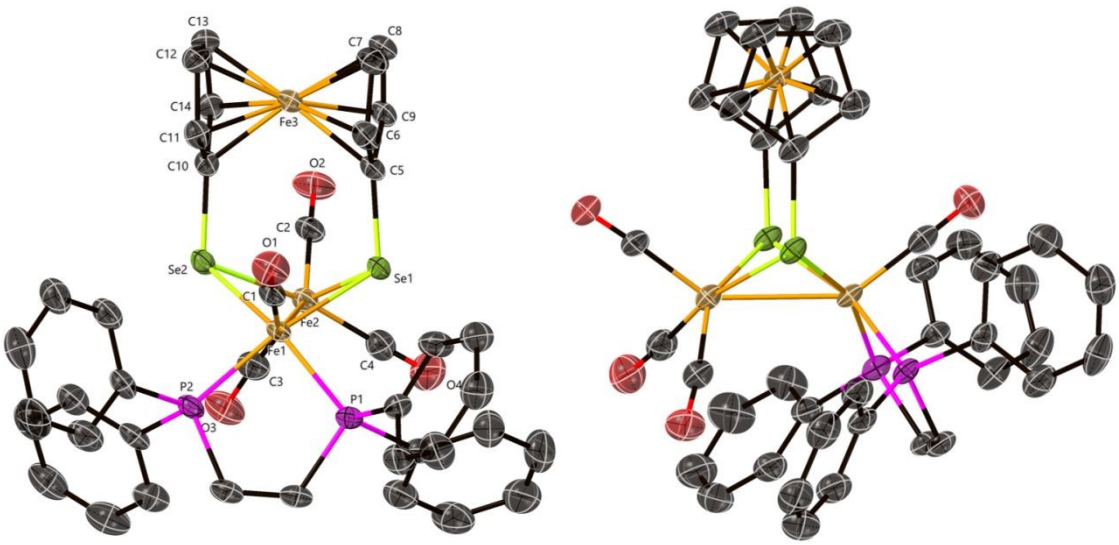

Fig. 2 Two views of the molecular structure (capped stick with hydrogen atoms removed for clarity) of **5**, looking down the diiron bond (right) and looking down ferrocene moiety (left). Selected bond distances (Å) and angles (°): Fe(1)–Fe(2) 2.6857(7), Fe(1)–P(1) 2.1989(9), Fe(1)–P(2) 2.1989(9), P(1)–Fe(1)–P(2) 86.55(3).

2.3. Synthesis of $[Fe_2(CO)_4\{\mu\text{-}E(\eta^5\text{-}C_5H_4)Fe(\eta^5\text{-}C_5H_4)E\}(\mu\text{-dppf})]$ (E = S (6) and Se (7))

Dppf is a flexible diphosphine[79-81] and we have previously shown that dppf-bridged $[Fe_2(CO)_4(\mu\text{-pdt})(\mu\text{-dppf})]^{2+}$ can catalytically oxidise H_2.[33] Our initial attempt to prepare $[Fe_2(CO)_4\{\mu\text{-Se}(\eta^5\text{-}C_5H_4)Fe(\eta^5\text{-}C_5H_4)Se\}(\mu\text{-dppf})]$ (E = S (**6**) and Se (**7**)), using conditions akin to those adopted for **4** and **5**, were unsuccessful. Dropwise addition of a THF solution of Me_3NO to a solution of **1** or **2** and 2.5 equivalents dppf at 45 °C led initially to the formation of pentacarbonyl species believed to be $[Fe_2(CO)_5\{\mu\text{-Se}(\eta^5\text{-}C_5H_4)Fe(\eta^5\text{-}C_5H_4)Se\}(\kappa^1\text{-dppf})]$ (for E = S, **Fig. S1**) and then the formation of the desired complexes **6** and **7** (for E = S, **Fig. S2**), which were isolated following workup (**Scheme 3**).

View Article Online
DOI: 10.1039/D6DT00946H

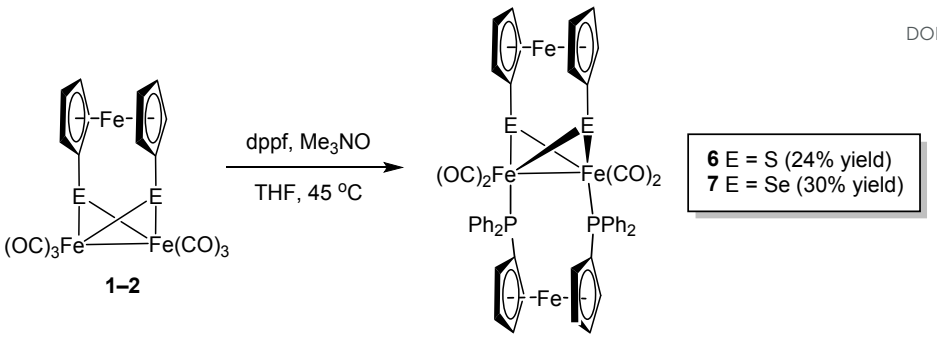

Scheme 3 Synthesis of $[Fe_2(CO)_4\{\mu\text{-}E(\eta^5\text{-}C_5H_4)Fe(\eta^5\text{-}C_5H_4)E)\}(\mu\text{-dppf})]$ (E = S (**6**) and Se (**7**)).

Both **6** and **7** exhibit an IR ν(CO) band pattern characteristic consistent with an $[Fe_2(CO)_4(\mu\text{-dithiolate})(\mu\text{-diphosphine})]$ complex, the absorption maxima in **7** being positively shifted by ca. 10 cm^{-1} (e.g., 1991 vs 1981 cm^{-1}) as compared to **6**. Both complexes exhibit a singlet in the $^{31}P\{^1H\}$ NMR spectrum, consistent with the symmetrical binding of dppf and for **7**, ^{77}Se satellites were observed. In the solid-state structure (see below) there are 16 non-equivalent ferrocenyl protons. The ^1H NMR spectrum of **7** is broad (**Fig. S3**), reflecting a fluxional process, and little information could be gleaned. The ^1H NMR spectrum of **6** was more informative, the cyclopentadienyl region (**Fig. 3**) consisting of eight signals of equal intensities, each assigned to a pair of protons. This observation suggests a fluxional process resulting in the equivalent sulfur centres, akin to that established in related bis(diphenylphosphino)methane (dppm) complexes, whereby the diphosphine undergoes a concerted double trigonal twist.[82]

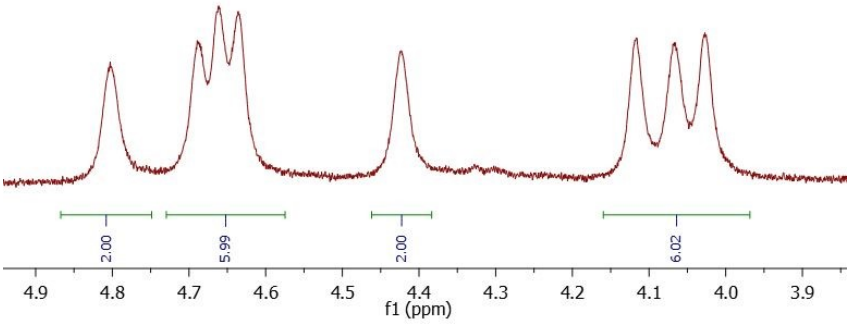

Fig. 3 Part of the ^1H NMR spectrum of **6** (CD_2Cl_2) revealing eight different ferrocenyl proton environments.

Crystals of **7** were grown by slow diffusion of hexanes into a concentrated CH_2Cl_2 solution, and the results of the X-ray crystallographic study (**Fig. 4**). The diiron separation in the core is ca. 0.1 Å longer than in **2** [2.5507 (5) in **2** vs. 2.6681 (12) Å in **7**], but similar to that of the dppv analogue, **5**. Unlike **5,** where the distance from the ferrocenyl Fe centre to the diiron bond is shorter than in parent **2**, for **7** it remains relatively unaffected [4.4401 (6) Å for **2**, 4.4538 (10) for **7**]. The static structure of **7** is similar to that of $[Fe_2(CO)_4(\mu\text{-pdt})(\mu\text{-dppf})]$,[33] the difference in their Fe–Fe bond lengths being *ca.* 0.05 Å. In **7** the distance between an iron centre from the Fe–Fe bond to the dppf iron atom is > 0.2 Å greater than the distance to the ferrocenyl bridgehead iron centre.

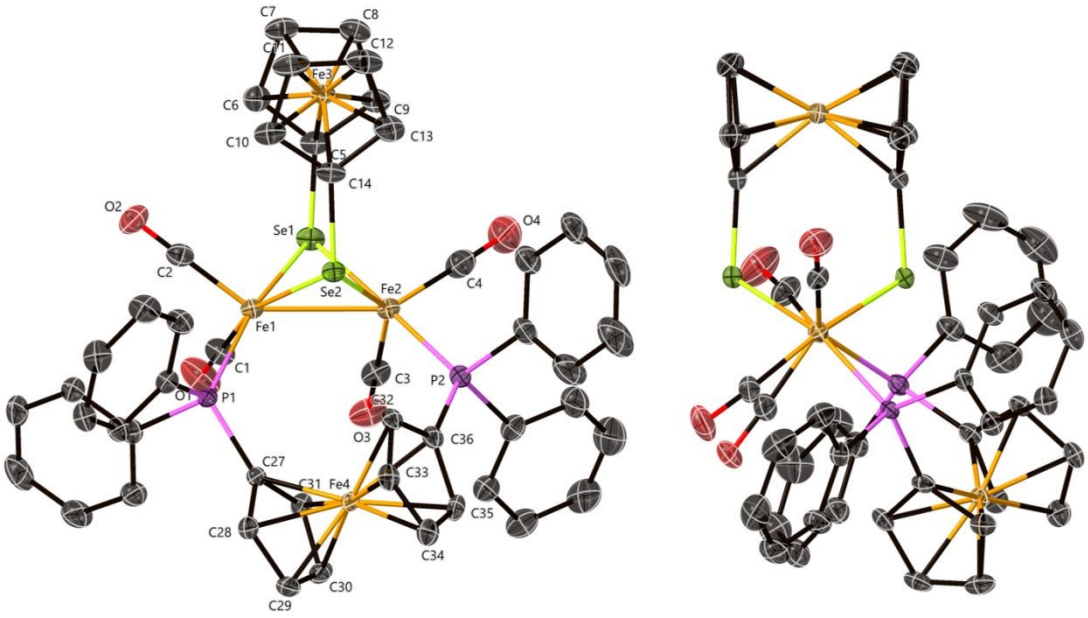

Fig. 4 Two views of the molecular structure of **7** (capped sticks with hydrogen atoms removed for clarity) of **7**, looking down the ferrocene moiety (left), and down the diiron bond (right). Selected bond distances (Å) and angles (°): Fe(1)–Fe(2) 2.6679(10), Fe(1)–P(1) 2.2520(12), Fe(2)–P(2) 2.2352(13), Fe(3)Fe(4) 8.069, Fe(3)–Fe(1) 4.424, Fe(3)–Fe(2) 4.454.

2.4. Probing oxidation chemistry by CV, IR SEC and preliminary DFT studies

We recently reported CV and IR SEC investigations of **1**–**2**.[45,46] Both show a quasi-reversible oxidation occurring at +0.14 (ΔE 110 mV) for **1** and +0.37 (ΔE 180 mV) for **2,** being characterized by ca. 15 cm^{-1} blue shifts in the IR ν(CO) spectral region and thus associated with a ferrocenyl-based one-electron process.[46] In such hexacarbonyl complexes, oxidation of

View Article Online
DOI: 10.1039/D6DT00946H

the carbonyl-bearing Fe_2S_2 centre is outside of the electrolyte potential window. Complexes **1** and **2** also undergo a quasi-reversible reduction at –1.81 and –1.56 V, respectively, being associated with addition of an electron to the Fe_2S_2 core. The quasi-reversibility appears to result from a structural change which leads to the formation of a bridging carbonyl, as proven by a new IR ν(CO) band at ca. 1715 cm^{-1}.

The CV of mono-substituted **3** in CH_2Cl_2 (**Fig. 5a**) shows a chemically reversible one-electron oxidation at $E_{1/2}$ = 0.30 V, some 70 mV less positive than the oxidation of **2**. The large value of ΔE_p (260 mV), which increases with the scan rate, is indicative of slow electron transfer, likely caused by a geometric rearrangement upon the oxidation of the ferrocenyl centre. Scanning to more positive potentials results in a large oxidation wave (not shown) and passivation of the electrode and thus little further insight could be gained. Unfortunately, though not unexpectedly,[49] oxidation of the Fe_2S_2 centre remains outside of the electrolyte potential window. Reduction of **3** occurs at –1.63 V and is irreversible over all scan rates, the large size of the reduction wave (as compared to the oxidation) suggesting that this multielectron processes likely corresponding to destruction of the parent structure.

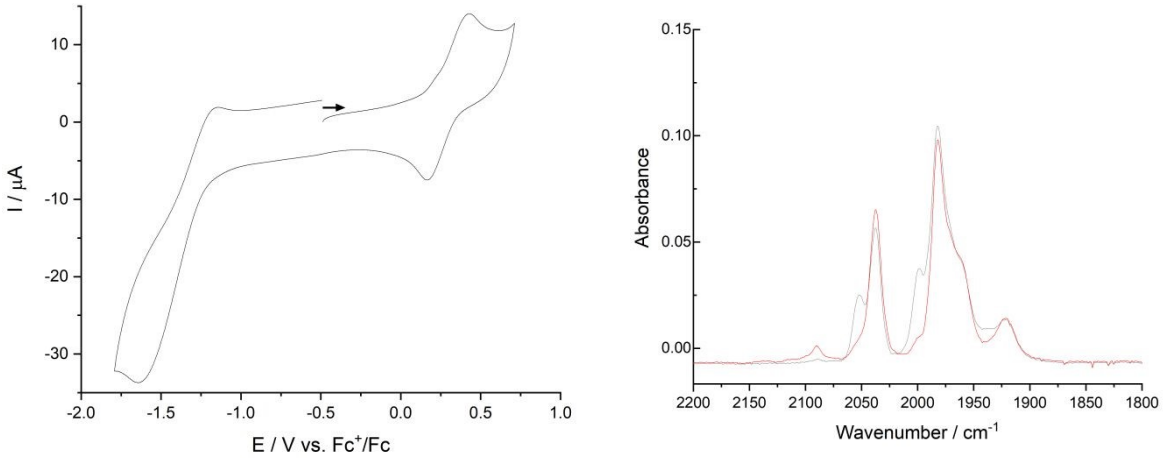

(a) (b)

Fig. 5 (a) CV of 1 mM **3** in CH_2Cl_2/TBAH at 0.1 V s^{-1} and (b) IR SEC of 1 mM **3** in CH_2Cl_2/0.1 M TBAH) showing (partial) oxidation to $\mathbf{3}^+$ (in red).

The assignment of the observable oxidation of **3** as ferrocenyl-based has been confirmed by IR SEC (**Fig. 5b**). which shows a *ca.* 15 cm^{-1} blue shift of the ν(CO) absorptions in agreement with the behaviour of oxidized **2**.[45] When the electrode potential was held

constant at the oxidation potential of **3** to observe full conversion to $\mathbf{3}^+$, ν(CO) bands assigned to $\mathbf{3}^+$ decreased in intensity and a new absorption appeared at 2090 cm^{-1} (**Fig. S4**), which possibly corresponds to adsorbed CO on the Pt-minigrid electrode.[83,84] This suggests that $\mathbf{3}^+$ is not stable and consequently further oxidation is accessible. Importantly, coordination of a single phosphine ligand does not move the oxidation of the Fe_2S_2 centre into the potential window of the dichloromethane electrolyte.

Disubstitution is expected to sufficiently lower the Fe_2S_2 oxidation potential to bring it within the potential window.[49] In CH_2Cl_2 (**Fig. 6a**), the oxidation chemistry of **5** is complicated. An electrochemically irreversible oxidation at 0.03 V is seen, which is independent of the scan rate over the range investigated. Two further oxidation events at 0.28 V and 0.45 V are also observed, the former having some reversibility, and both being dependent on the scan rate, with faster scan rates favouring the third event and slower scan rates the second one. In MeCN (**Fig. 6b** and **Fig. S5**) only two oxidation events are observed at 0.11 V and 0.30 V, although the position of these is dependent on scan rate. Changes to the oxidation chemistry in this solvent suggest that solvent coordination may be occurring. Complex **4** also exhibits varying redox chemistry in these solvents (**Figs S6–S7**). In MeCN (**Fig. S6**), two irreversible oxidation events are observed at $E_{p,a}$ = 0.10 V and 0.44 V, whereas in CH_2Cl_2 several irreversible, scan-rate dependent processes occur which cannot easily be distinguished from one another.

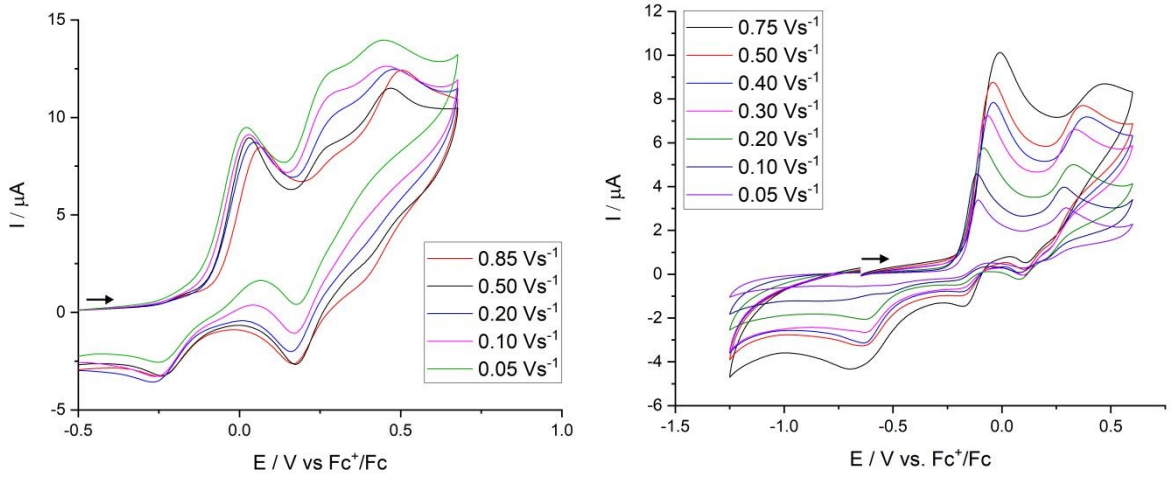

Fig. 6 CVs of 1 mM **5** at varying scan rates (normalised for scan rate) in (a) CH_2Cl_2/TBAH and (b) MeCN/TBAFP.

View Article Online
DOI: 10.1039/D6DT00946H

To investigate the nature of the species formed upon their oxidation, we performed IR SEC of **4**–**5** in CH_2Cl_2, initially focusing on **4** due to its higher solubility (**Fig. 7**). Initial oxidation of **4** results in formation of a new species in which the highest frequency ν(CO) band is shifted by ca. 50 cm^{-1}, indicative of oxidation at the Fe_2S_2 core (**Fig. 7a**). Holding the potential at the maxima of the first oxidation wave results in conversion to a species in which the largest ν(CO) wavenumber is shifted by a further 11 cm^{-1} (**Fig. 7b**), being consistent with oxidation of the ferrocenyl centre to give a dication. At higher potentials, this species undergoes further oxidation, being accompanied by an 18 cm^{-1} blue shift in the ν(CO) wavenumbers (**Fig. 7c**). It is not clear where this third oxidation takes place, but we suggest that it is second oxidation of the Fe_2S_2 moiety to afford a diferrous diiron centre.[85-88] Importantly, while the CV shows that these processes are electrochemically irreversible, they are chemically reversible. Thus, upon reversing the potential scan direction, **4** is reformed. For **5** (**Fig. S8**), individual processes could not be resolved; however, observations broadly similar to **4** were made. A mixture of species form following the first oxidation; an absorbance at 1995 cm^{-1} being like that observed for the initial product of oxidation of **4**, whilst the overall Δν(CO) of 64 cm^{-1} and number of bands suggests that the dication may also be produced. Upon scanning to higher potentials, an additional oxidation event is reached, which shows a further 10 cm^{-1} ν(CO) hypsochromic shift. These results suggest that the first oxidation of **4**–**5** is Fe_2S_2 based, and the second oxidation is localised at the bridging ferrocene centre. The nature of the third oxidation is unresolved but, given the chemical reversibility, we suggest it occurs at the Fe_2S_2 centre to afford a diferrous complex.

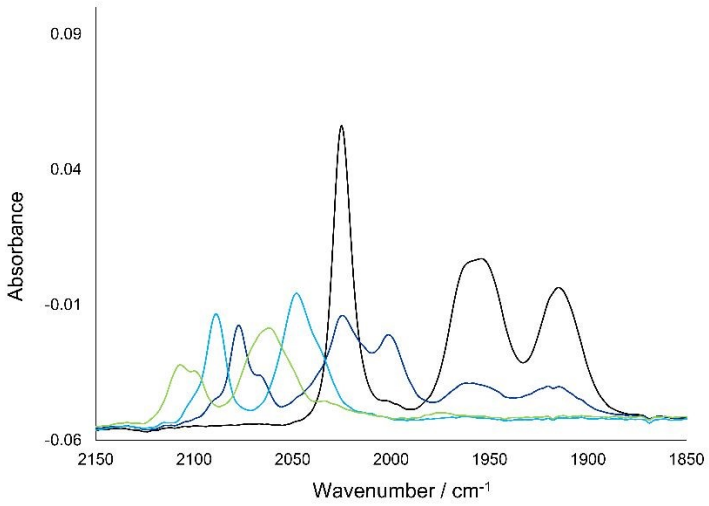

Fig. 7 IR SEC of **4** in 0.1 M TBAH/CH_2Cl_2 showing (i) black trace for **4** and dark blue for first oxidation product $\mathbf{4}^+$, (ii) generation of dication $\mathbf{4}^{2+}$ (light blue trace), (iii) third, unassigned oxidation (green trace)

View Article Online
DOI: 10.1039/D6DT00946H

The more complex nature of the CVs of **4**–**5** may be a result of electron-transfer processes, i.e. interconverting the initially formed Fe_2(I)/(II)-Fc(II) configuration in [**4**–**5**]$^+$ with an Fe_2(I)/(I)-Fc(III) i.e. electron-transfer from the ferrocene-dithiolate to the diiron centre. To better understand the oxidation of **4**–**5** and support the assignment of the products, we carried out DFT calculations on **5** and **5**$^+$. For **5** (**Fig. 8**) the HOMO is localised at the Fe_2 centre, while HOMO–1 is localised at the ferrocenyl centre.

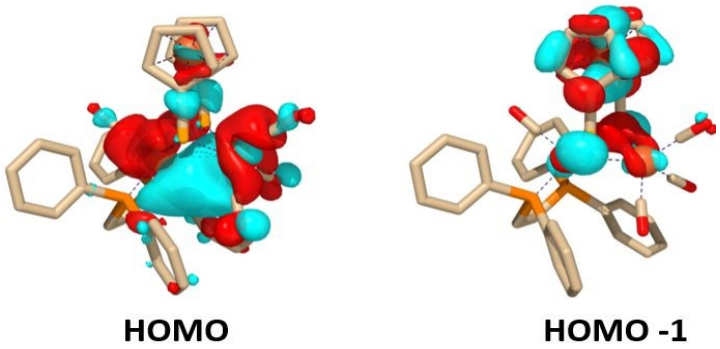

Fig. 8 DFT-calculated HOMO and HOMO–1 of **5**.

Thus, while initial oxidation at the diiron centre is predicted, we sought to probe the lowest energy conformations of **5**$^+$ to understand if a significant structural and/or electronic rearrangement occurs. DFT calculations on **5**$^+$ identified two possible structures, which we label **Cation_1** and **Cation_2** (**Fig. 9**), with an energy difference of ca. 1.3 kcal in favour of **Cation_2**. In **Cation_1**, the spin density is delocalized across the Fe_2 centre, and all carbonyls remain terminally bonded, while for **Cation_2** oxidation is localised at the dppv-substituted iron centre and results in the formation of the semi-bridging carbonyl, the so-called rotated state. Formation of a semi-bridging carbonyl upon oxidation of Fe(I)Fe(I) dithiolate complexes is commonly observed, the unique carbonyl normally appearing below 1900 cm^{-1} in the IR spectrum.[44,89–92] As seen by IR SEC, oxidation of **4** to **4**$^+$ does not generate a semi-bridging carbonyl (**Fig. 7a**); rather, the pattern of IR bands remains similar to that for the unoxidized species. Thus, it appears that (on the timeframe of the IR SEC experiment at least) oxidation of **4** (and **5**) affords an all terminal-CO bound cation, consistent with **Cation_1**. An explanation for this is that the rigid nature of dithiolate group leads to a high activation barrier for the Fe(CO)(diphosphine) rotation required to give a semi-bridging carbonyl. We note that some related cations, including $[Fe_2(CO)_4\{\kappa^2\text{-}(Ph_2PCH_2)_2N(R)\}(\mu\text{-pdt})]^+$, adopt a non-rotated

View Article Online
DOI: 10.1039/D0DT00946H

structure.[41,42] Importantly, neither cation has a significant contribution of spin density on the ferrocene centre, thus discounting a facile electron-transfer from the latter to the diiron centre.

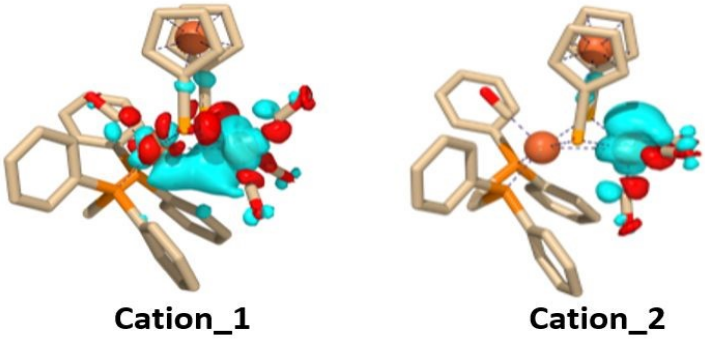

Fig. 9 DFT-predicted localisation of the spin density in isomers of $\mathbf{5}^{+}$.

We next studied dppf-bridged **6**–**7** which contain three different (potentially) oxidisable iron centres. For comparison, we briefly review CVs of $[Fe_2(CO)_4(\mu\text{-pdt})(\mu\text{-dppf})]$[33] and $[Fe_2(CO)_6\{\mu\text{-E}(\eta^5\text{-}C_5H_4)Fe(\eta^5\text{-}C_5H_4)E)\}]$.[45,46] Dppf-bridged $[Fe_2(CO)_4(\mu\text{-pdt})(\mu\text{-dppf})]$ shows two oxidative processes in MeCN, a reversible oxidation at 0.05 V (ΔE = 60 mV) and a quasi-reversible oxidation at 0.68 V, associated with oxidation of the diiron core and the bridging ferrocenyl centre, respectively. The enhanced reversibility of the oxidations in MeCN vs CH_2Cl_2 likely represents solvent coordination at the generated cationic centres.[42] We first studied the oxidative chemistry of **6** in CH_2Cl_2 due to its good solubility. It shows a quasi-reversible first oxidation at $E_{1/2}$ = 0.05 (ΔE = 150 mV when v = 0.1 Vs^{-1}) (**Fig. S9**). At higher potentials, a second irreversible oxidation is seen at ca. 0.22 V, but the subsequent reduction of the species generated is complex and was not explored further. As for similar complexes, in MeCN the redox behaviour is simplified. Thus, **6** shows a quasi-reversible oxidation at $E_{1/2}$ = 0.09 V (ΔE_p = 90 mV when v = 0.5 Vs^{-1}) and two further irreversible oxidations at $E_{p,a}$ = 0.44 V and 0.64 V (**Fig. 10**). The selenium-analogue **7** shows a similar behaviour in CH_2H_2, undergoing a quasi-reversible oxidation at $E_{1/2}$ = 0.03 V (ΔE = 90 mV) (**Fig. 11a**) and two further electrochemically irreversible oxidations at $E_{p,a}$ = 0.40 V and 0.53 V (**Fig. 11b**), occurring at slightly less positive potentials than those for **6**. No reduction chemistry was accessible for either **6** or **7**. Oxidation of the diiron centre in **6** occurs at a similar potential to that in $[Fe_2(CO)_4(\mu\text{-pdt})(\mu\text{-dppf})]$,[33] showing that the electronic properties of the two thiolate bridges are similar. Thus, we suggest the order of the oxidation of **6** and **7** is likely: (i) initial

View Article Online
DOI: 10.1039/D6DT00946H

oxidation of the diiron centre, (ii) second oxidation centred at the ferrocene of the dithiolate bridge, and (iii) third oxidation on the dppf-ligand.

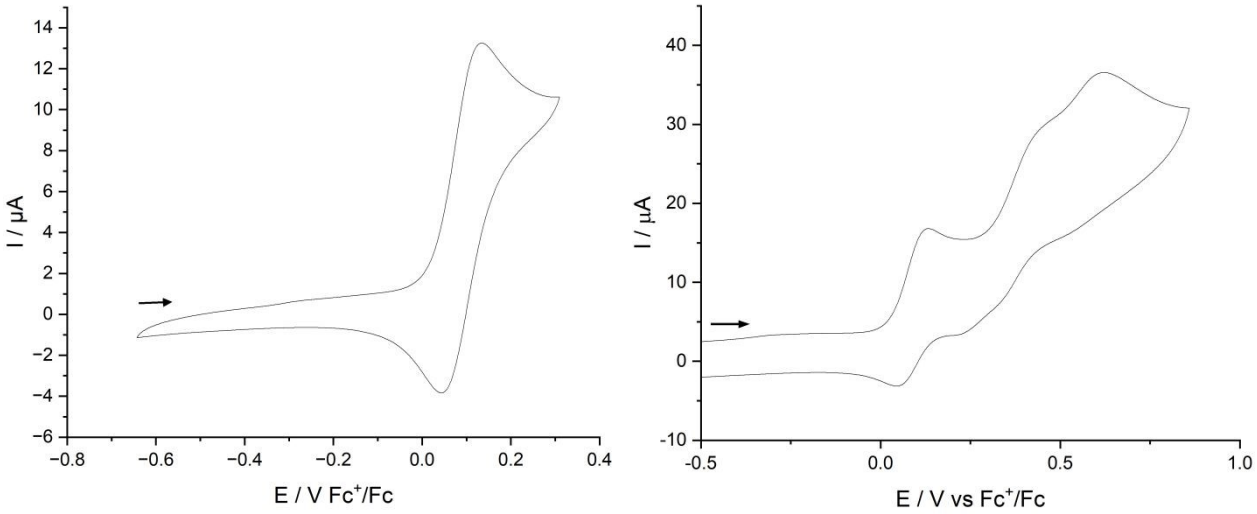

(a) (b)

Fig. 10 CVs of 1 mM **6** in 0.1 M TBAH/MeCN showing (a) the quasi-reversible first oxidation; $\nu = 0.5$ Vs^{-1}, and (b) all three observed oxidation events.

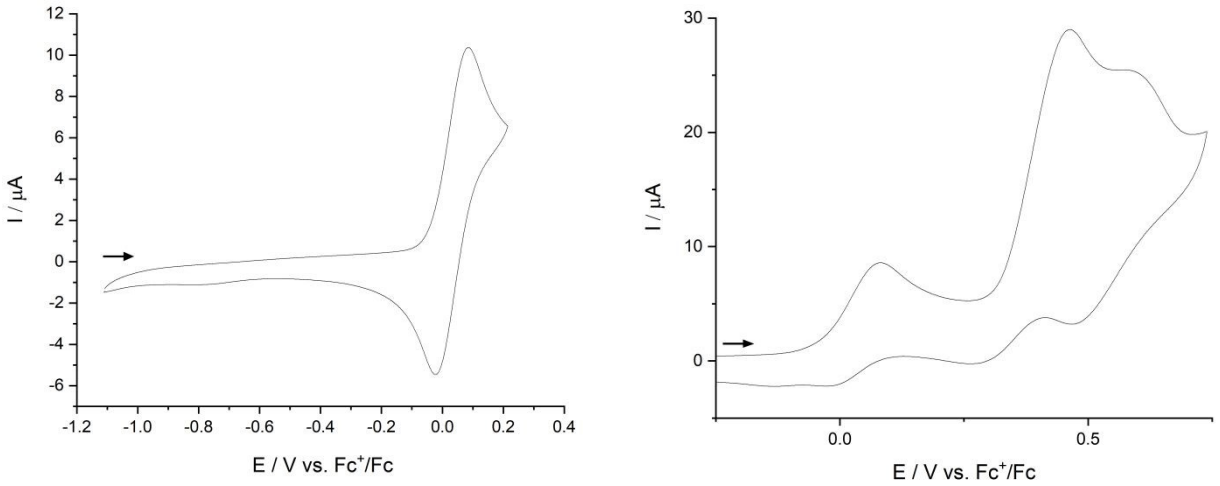

(a) (b)

Fig. 11 CVs of 1 mM **7** in 0.1 M TBAH/CH_2Cl_2 showing (a) the quasi-reversible first oxidation; $\nu = 0.5$ Vs^{-1}, and (b) all three observed oxidation events.

These suppositions can (in theory at least) be explored by IR SEC. Unfortunately, the insolubility of oxidation products of **6** prevented its detailed study, but oxidation products of **7** are more soluble in CH_2Cl_2 enabling IR monitoring of the process (**Fig. 12**). The species $\mathbf{7}^+$

View Article Online
DOI: 10.1039/D0DT00946H

generated after the first oxidation event (marked **Δ**) shows a 48 cm^{-1} shift in the highest-frequency ν(CO) band, consistent with oxidation occurring primarily at the Fe_2S_2 centre. By way of comparison, oxidation of $[Fe_2(CO)_4(\mu\text{-pdt})(\mu\text{-dppf})]$[43] shows two events in MeCN, the first being associated with a large hypsochromic shift of ca. +60 cm^{-1}.[43] Unfortunately, we were unable to identify individual products from the second and third oxidation waves. A species exists in solution (marked ϕ) where the highest-frequency ν(CO) band is blue shifted by a further 107 cm^{-1}. Assignment is not straightforward but based on the behaviour of **5** and $[Fe_2(CO)_4(\mu\text{-pdt})(\mu\text{-dppf})]$.[43] We expect both ferrocenyl groups to undergo oxidation. However, given that oxidation of a bridging ferrocenyl centre results in a ν(CO) shift of only ca. 15 cm^{-1},[46] it seems that second oxidation of the Fe_2 core may be involved to achieve the large ν(CO) band shift of 107 cm^{-1}.

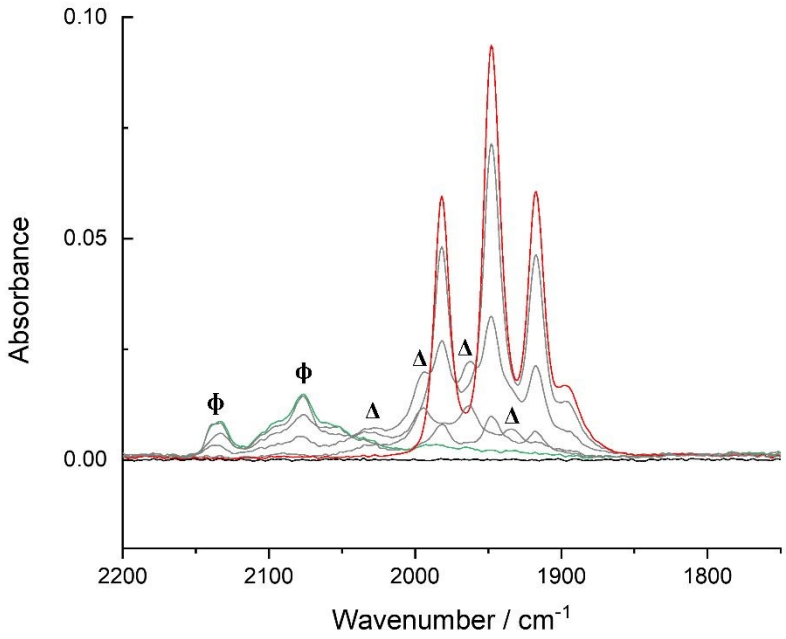

Fig. 12 IR SEC of 1 mM **7** (red trace) in 0.1 M TBAH/CH_2Cl_2. The product of the first oxidation is labelled as **Δ**, and further oxidations (green trace) as **ϕ**.

Calculations on **7** and $\mathbf{7}^+$ are largely in agreement with conclusions drawn from experimental measurements. Closed-shell DFT calculations suggest that **7** has an Fe_2-based HOMO and thus initial oxidation would be expected to be primarily localised there. Cation $\mathbf{7}^+$ is predicted to have a semi-bridging CO ligand with spin density localised predominantly at the $Fe(CO)_3$ centre (**Fig. 13**), but some dppf ferrocenyl character, which might account for the smaller than expected Δν(CO) upon oxidation of **7** to $\mathbf{7}^+$.

View Article Online
DOI: 10.1039/D6DT00946H

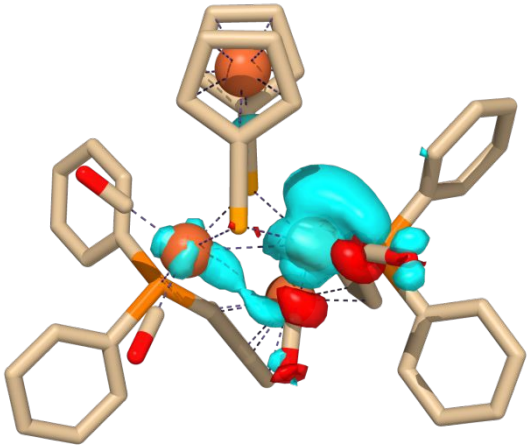

Fig. 13 Calculated spin density distribution in $\mathbf{7}^{+}$.

2.5. Summary of oxidation results

Table 1 gives a summary of the oxidation chemistry of **1**–**7** in CH_2Cl_2. Changes to the oxidation potential of the ferrocene centre of the dichalcogenolate bridge are relatively minor, but measurable, upon phosphine substitution of the diiron centre. Thus, oxidation of diseleno-hexacarbonyl **2** is shifted to lower electrode potentials by ca. 0.07 V upon successive CO substitutions to afford **3** and **5** respectively, consistent with a small increase in electron density at the ferrocene centre. The IR SEC studies provide support for the oxidation of the dichalcogenolate bridge in **1-3**. The hexacarbonyl-supported diiron centre is relatively electron-deficient and its oxidation is outside of the accessible range. As noted in related complexes,[50] substitution of a single carbonyl does not bring the oxidation into the potential window. However, upon substitution of two carbonyls, not only does oxidation of the Fe_2 centre shift to a significantly lower electrode potential, but it also becomes easier to oxidise than the ferrocene-dichalcogenolate centre. Oxidation of the diiron centre in chelate complexes **4**–**5** (in CH_2Cl_2) is irreversible, which is normally associated with a significant structural change resulting from formation of a semi-bridging carbonyl upon oxidation.[89-92] Frustratingly, we could not identify such a species via IR SEC studies, although we note that such bands are often of low intensity.[44] We suggest that the rigidity of the dichalcogenolate bridge makes formation of such a species unfavourable, and another structural rearrangement occurs to afford a adopt a non-rotated cationic structure as has

View Article Online
DOI: 10.1039/D0DT00946H

previously been noted.[41,42] DFT studies suggest that such a species may be akin to the calculated structure of **Cation_1** (**Fig. 9**).

Table 1. Oxidation potentials for **1**–**7** (in CH_2Cl_2[a] or MeCN[b]).

Compound	$E_{p,a}^{1st}$ /V	$E_{p,a}^{2nd}$ /V	$E_{p,a}^{3rd}$ /V	Ref
1[a]	0.14 (ΔE 110mV) Fc			45
2[a]	0.37 (ΔE 180mV) Fc			46
3[a]	0.30 (ΔE 260mV) Fc			
4[a]	0.02 (irrev) Fe_2	0.22 (ΔE 110mV) Fc	0.45 (irrev)	
5[a]	0.03 (irrev) Fe_2	0.23 (ΔE 90mV) Fc	0.46 (irrev)	
6[b]	0.09 (ΔE 90mV) Fe_2	0.44 (irrev) Fc	0.64 (irrev) PFcP	
7[a]	0.03 (ΔE 90mV) Fe_2	0.40 (irrev) Fc	0.53 (irrev) PFcP	

In dppf-bridged **6**–**7** there are three separate oxidisable centres and for both **6** (in MeCN) and **7** (in CH_2Cl_2) three oxidation events were noted. The first oxidation is quasi-reversible. It likely occurs at the diiron centre, but for **7,** the slightly smaller than expected (see below) Δν(CO) of 48 cm^{-1} accompanying this oxidation suggests it is (at least in part) delocalised at one of the ferrocene centres. DFT calculations show that a cation $\mathbf{7}^+$ with a semi-bridging carbonyl is thermodynamically favoured but no such species was clearly observed by IR SEC. DFT calculations also suggest that some of the positive charge in $\mathbf{7}^+$ is localised on the dppf ligand. Thus, there appears to be some evidence for communication between redox centres in **6**–**7**. This might also account for the higher-than-expected potential of the second oxidation event. Thus, from studies on **1**–**5** we might expect oxidation of the ferrocene-dichalcogenolate bridge to occur around 0.3 V; however, for both **6** and **7** it is seen at ca. +0.1 V higher. This provides further evidence for the communication between redox centres and might suggest partial oxidation of the dichalcogenolate bridge at the first oxidation event. The irreversible nature of the second oxidation necessarily makes interpreting further redox events tentative, but for both a third oxidation event is seen, at 0.64 (for **6**) and 0.53 V (for **7**). The IR SEC studies of **7** do not allow us to separate the second and third oxidation events. However, the large hypsochromic shift (ca. 100 cm^{-1}) upon further oxidation of $\mathbf{7}^+$ suggests that there is a significant Fe_2 contribution, providing further evidence of electronic communication between the three oxidation centres.

View Article Online
DOI: 10.1039/D6DT00946H

3 Conclusions

In this contribution, we have studied the phosphine-substitution chemistry of ferrocene-dichalcogelate complexes, $[Fe_2(CO)_6\{\mu\text{-}E(\eta^5\text{-}C_5H_4)Fe(\eta^5\text{-}C_5H_4)E)\}]$ (E = S, Se) (**1**–**2**) with the aim of tuning the oxidation potential of the Fe_2 centre, whilst (effectively) leaving that of the ferrocene centre unchanged. The first thing to highlight is the extreme difficulty in preparing and purifying such phosphine-substituted derivatives which contrasts greatly with the chemistry of [FeFe]-H_2ase biomimics with flexible linking units, such as $[Fe_2(CO)_6(\mu\text{-pdt})]$.[50] This difference likely results from the different accessible mechanistic pathways with substitution of $[Fe_2(CO)_6(\mu\text{-pdt})]$[50,69,93] and non-bridged dithiolate complexes $[Fe_2(CO)_6(\mu\text{-SR})_2]$[68,94] occurring via an associative pathway,[50,69] such a state being rendered inaccessible via the rigid ferrocene-dithiolate unit. Thus, a dissociative substitution pathway must be used, with Me_3NO acting as the decarbonylation agent, and THF as the solvent, probably proceeding via lightly stabilised intermediates $[Fe_2(CO)_5(THF)\{\mu\text{-}E(\eta^5\text{-}C_5H_4)Fe(\eta^5\text{-}C_5H_4)E)\}]$. Replacement of the THF by phosphine requires a higher temperature and thus adding the phosphine at low temperatures and then warming is an effective strategy. For the diphosphine complexes, as we used only one equivalent of Me_3NO, the second substitution must be thermally affected and the relatively good yield (60%) of $[Fe_2(CO)_4\{\mu\text{-}Se(\eta^5\text{-}C_5H_4)Fe(\eta^5\text{-}C_5H_4)Se)\}(\kappa^2\text{-dppv})]$ (**5**) suggests that the monodentate analogue has reasonable thermal stability. We have found in related chemistry[43] that the challenge in preparing μ-dppf complexes is in minimising the initial formation of the dppf-bridged tetra-iron complexes. This is relatively easy here as it can simply be controlled by the amount of Me_3NO added since the associative (none Me_3NO assisted) route is not accessible. Thus, while yields of dppf adducts **6**–**7** were not high, reactions were reproducible and relatively easy to carry out.

Armed with a small selection of phosphine-substituted derivatives of **1**–**2** our aim was to investigate their oxidation chemistry by CV and IR SEC experiments. The strategy of tuning the oxidation potential of the Fe_2 centre upon successive carbonyl-to-phosphine substitution is well-established,[50] and our results in this regard were as expected (**Table 1**). Thus, upon replacement of one carbonyl, oxidation potential of the ferrocene-dichalcogenolate centre was slightly reduced, but oxidation of the Fe_2 centre was still not within the CV window. Replacement of the second carbonyl, in either chelate (dppv) or bridged (dppf) complexes reduced the oxidation potential of the Fe_2 centre to bring it below that of the ferrocene-dichalcogenolate. This is broadly

View Article Online
DOI: 10.1039/D0DT00946H

supported by IR SEC studies, although hypsochromic shifts are slightly lower than in related edt and pdt complexes suggesting some degree of electronic communication between the various redox centres. DFT studies on both dppv and dppf complexes suggest that oxidation of the diiron centre should result in formation of thermodynamically stable cation(s) with a semi-bridging carbonyl, but this is not observed by IR SEC. Reasons for this are not immediately apparent, but it may be that the rigidity of the ferrocene-dichalcogenolate backbone does not allow for a low energy pathway to such species. Dppf complexes, which contain three oxidisable centres, show three oxidation events by CV and IR SEC studies show that the first oxidation is primarily diiron centred. Based on a comparison of oxidation potentials of related dppf complexes it is suggested that the second oxidation is primarily at the ferrocene-dichalcogenolate centre, and the third at the dppf ligand, but their proximity makes this impossible to show by IR SEC. Indeed, the large hypsochromic shifts following oxidation of $\mathbf{7}^{+}$ suggest that there may also be some further oxidation of the Fe_2 centre during these events.

4 Experimental section

All reactions were carried out using standard Schlenk-line techniques under N_2 using anhydrous solvents. Work-up was done in air using standard bench reagents. Phosphines were purchased from Santa Cruz Biotech (Texas, USA) or from Aldrich (Gillingham, UK) and were used without further purification. Complexes **1**–**2** were prepared as previously reported.[46,47] NMR spectra were recorded on a BrukerAvance 400 MHz Ultrashield NMR spectrometer (Coventry, UK) and referenced internally to residual solvent peaks or H_3PO_4. High resolution electron spray ionisation mass spectra were recorded on a Bruker Daltronics Esquire 3000 spectrometer (Coventry, UK) by Dr Lisa Haigh (Imperial College). FTIR spectra were recorded with a IRAffinity-1S Shimadzu spectrophotometer (Milton Keynes, UK) in a solution cell fitted with calcium fluoride plates, subtraction of the solvent absorptions being achieved by computation.

4.1 Syntheses and characterisation

$[Fe_2(CO)_5\{\mu\text{-}Se(\eta^5\text{-}C_5H_4)Fe(\eta^5\text{-}C_5H_4)Se\}(Ph_2P\text{-}p\text{-}tolyl)]$ (3)

A solution of **2** (200 mg, 0.32 mmol) in MeCN (7 mL) was cooled to ca. –20 °C in an ice/NaCl bath and $Me_3NO{\cdot}2H_2O$ (34 mg, 0.3 mmol, 0.95 equiv.) was added and the solution stirred for 20 min. Then, PPh_2(*p*-tolyl) (89 mg, 0.32 mmol) was added, and the solution allowed to warm to room temperature and stirred for 3 h. Solvent was removed under reduced pressure and the product purified on a 10 cm long silica gel column (hexane/CH_2Cl_2, 4:1 v/v). Following elution of unreacted **2** a second brown fraction gave **3** as a black solid (103 mg, 37 %). ^{1}H NMR (CD_2Cl_2) δ 7.68 – 7.21 (m, 14H, Ar), 4.43 (s, 2H, Cp), 4.34 (s, 2H, Cp), 4.09 (m, 4H, Cp), 2.39 (s, 3H, Me). ^{31}P{^{1}H} NMR (CD_2Cl_2) δ 63.9 (s) ppm. IR (CH_2Cl_2) ν(CO): 2037, 1982, 1962, 1920 cm^{-1}. ESI(+)MS: *m/z* calcd for ($C_{34}H_{25}Fe_3O_5PSe_2$): 871.78; Found $[M + H]^+$ = 872.7929.

[$Fe_2(CO)_4${μ-S(η^5-C_5H_4)Fe(η^5-C_5H_4)S)}(κ^2-dppv)] (4)

Prepared as for **5** (see below for details). Yield (3.6 %). ^{1}H NMR ($CDCl_3$) δ 8.09 – 7.33 (m, 22 H, Ar + CH), 4.74 (s, 2H, Cp), 4.52 (s, 2H, Cp), 4.06 (s, 4H, Cp). ^{31}P{^{1}H} NMR ($CDCl_3$) δ 81.2, 80.1 ppm. IR (CH_2Cl_2) ν(CO): 2025, 1956, 1914 cm^{-1}.

[$Fe_2(CO)_4${μ-Se(η^5-C_5H_4)Fe(η^5-C_5H_4)Se)}(κ^2-dppv)] (5)

Complex **2** (100 mg, 0.16 mmol) and dppv (64 mg, 0.16 mmol) were dissolved in dry, degassed THF (5 mL) under N_2 and cooled to ca. –20 °C in an ice/NaCl bath. $Me_3NO{\cdot}2H_2O$ (17.8 mg, 0.16 mmol) was added under N_2 and the solution stirred for 20 min. The solution was then heated to 40 °C and stirred for 1 h until the IR spectrum showed complete loss of **2**. Following removal of the solvent the crude mixture was washed with hexanes (3 × 20 ml), dissolved in a minimum amount of CH_2Cl_2 and precipitated by addition of hexanes (100 ml). Filtration gave the pure product as a dark purple/brown powder (93 mg, 60 %). ^{1}H NMR (CD_2Cl_2) 8.06 – 7.27 (m, 22H, Ar + CH), 4.65 (s, 2H, Cp), 4.47 (s, 2H, Cp), 4.12 (s, 4H, Cp); ^{31}P{^{1}H} NMR (CD_2Cl_2) δ 84.3 (s) ppm; IR (CH_2Cl_2) ν(CO): 2017vs, 1949s, 1911 cm^{-1}. ESI(+)MS: *m/z* calcd for ($C_{40}H_{30}Fe_3O_4P_2Se_2$): 963.80; Found $[M]^+$ = 963.8024.

[$Fe_2(CO)_4${μ-S(η^5-C_5H_4)Fe(η^5-C_5H_4)S)}(μ-dppf)] (6)

A THF solution of $Me_3NO{\cdot}2H_2O$ (17.8 mg, 0.16 mmol) was added to a pre-warmed solution of **1** (85 mg, 0.16 mmol) and dppf (222 mg, 0.4 mmol) at 45 °C. This was stirred at 45 °C for 30 min until the IR spectrum showed complete loss of **1**. The product was purified by prep TLC (hex: CH_2Cl_2, 55:45) and collected as the main brown band as soon as separation

View Article Online
DOI: 10.1039/D0DT00946H

from unreacted dppf (first band) and degraded material (baseline) had taken place. Removal of solvent under reduced pressure gave **6** as a brown powder (37 mg, 24%). ^{1}H NMR ($CDCl_3$) δ 8.00 (s, 4H, Ar), 7.54 (s, 4H, Ar), 7.33 (s, 12H, Ar), 4.71 (s, 2H, Cp), 4.60 (s, 2H, Cp), 4.57 (s, 2H, Cp), 4.55 (s, 2H, Cp), 4.34 (s, 2H, Cp), 4.03 (s, 2H, Cp), 3.98 (s, 2H, Cp), 3.94 (s, 2H, Cp); ^{31}P{^{1}H} NMR (CD_2Cl_2) 49.3 (s) ppm; IR (CH_2Cl_2) ν(CO): 1991s, 1954vs, 1924s, 1903w cm^{-1}. ESI(+)MS: m/z calcd for ($C_{48}H_{36}Fe_4O_4P_2S_2$): 1025.89; Found $[M]^+$ = 1025.8972, $[M + H]^+$ = 1026.9004.

[$Fe_2(CO)_4${μ-Se(η^5-C_5H_4)Fe(η^5-C_5H_4)Se}(μ-dppf)] (7)

A THF solution of $Me_3NO{\cdot}2H_2O$ (17.8 mg, 0.16 mmol) was added to a pre-warmed solution of **2** (100 mg, 0.16 mmol) and dppf (222 mg, 0.4 mmol) at 45 °C. The solution was stirred at 45 °C for 30 min until the IR spectrum showed complete consumption of **2**. The product was purified on a 10 cm silica gel column (hexane/CH_2Cl_2, 5:3 v/v) performed rapidly under positive pressure (N_2) with the product being collected as the main brown fraction. *The product is not stable on silica for more than a few minutes so this step must be performed rapidly.* Removal of the solvent under reduced pressure gave **7** as a dark brown crystalline powder (51 mg, 30%). XRD quality crystals were grown from a CH_2Cl_2 solution layered with hexanes. ^{1}H NMR (CD_2Cl_2) δ 8.41 (s, 4H, Ar), 7.60 (s, 4H, Ar), 7.45 (s, 12H, Ar), 4.98 (s, 2H, Cp), 4.61 (s, 8H, Cp), 4.36 (s, 2H, Cp), 4.21 (s, 2H, Cp), 4.14 (s, 2H, Cp). ^{31}P{^{1}H} NMR (CD_2Cl_2) δ 53.2-53.7 (br) ppm. IR (CH_2Cl_2) ν(CO): 1981s, 1948vs, 1916s, 1895w cm^{-1}. ESI(+)MS: *m/z* calcd for ($C_{48}H_{36}Fe_4O_4P_2Se_2$): 1121.78; Found $[M + H]^+$ = 1122.7788.

4.2 CV and IR SEC

Electrochemistry was carried out in anhydrous degassed acetonitrile or dichloromethane solutions using 0.1 M TBAH (tetrabutylammonium hefafluorophosphate, recrystallized and carefully dried) as the supporting electrolyte. Unless otherwise stated, the working electrode was a 3 mm diameter glassy carbon electrode that was polished with diamond slurry. The counter electrode was a Pt wire and the quasi-reference electrode was a silver wire or Pt electrode. All CVs were referenced to the $Fc^{+/0}$ redox couple. An Autolab Interface6 potentiostat was used for electrochemical measurements. IR SEC was performed with a Bruker Vertex 70v FT-IR spectrometer (Coventry, UK) equipped with a DTLaGS detector. The SEC experiment was recorded using thin-layer cyclic voltammetry (TL-CV) with an OTTLE cell,

View Article Online
DOI: 10.1039/D6DT00946H

an EmStat3+ (PalmSens) potentiostat and the PSTrace 4.2 software. The OTTLE cell[95] (Reading, UK) was equipped with a Pt minigrid-working electrode, a platinum minigrid counter electrode, an Ag-wire pseudo-reference electrode and CaF_2 windows. IR SEC samples contained 0.3 M supporting electrolyte and 1 mM analyte.

4.3 Computational Methodology

The DFT calculations reported in this chapter were done with the ORCA program package.[96] The structures were calculated using the molecular structure as a base. The structures of the cations were calculated from the optimized structures of the neutral species with additional electron(s). The geometry optimizations were carried out at the B3LYP level of DFT.[97]

4.4 Crystallography

Single-crystal X-ray diffraction data for **5** (CCDC 2548459) and **7**.CH_2Cl_2 (CCDC 2548460) were collected at 150(1) K using an Agilent Oxford Diffraction SuperNova (Oxford, UK) equipped with a microfocus Cu Kα X-ray source, a Cryojet5®, and an Atlas CCD detector using the CrysAlisPro software at University College London. The structures were solved using SHELXT[98] and refined using SHELXL[99] both of which were operated from within either the Oscail[100] or 4[101] software packages. Crystallographic data were deposited with the Cambridge Data Centre with deposition numbers and important crystallographic data being given in **Table S1**.

Acknowledgements

We thank King's College London for funding including the provision of a PhD studentship to GRFO. IR SEC measurements in Reading were sponsored by Spectroelectrochemistry Reading (spinout of SCFP led by FH).

Declaration of Competing Interest

The authors declare no competing interest.

View Article Online
DOI: 10.1039/D6DT00946H

References

1 Nicolet, Y.; Piras, C.; Legrand, P.; Hatchikian, C. E.; Fontecilla-Camps, J. C. Desulfovibrio desulfuricans iron hydrogenase: the structure shows unusual coordination to an active site Fe binuclear center. *Structure* **1999**, *7*, 13-23.

2 Peters, J. W.; Lanzilotta, W. N.; Lemon, B.; Seefeldt, L. C. X-ray crystal structure of the Fe-only hydrogenase (CpI) from Clostridium pasteurianum to 1.8 angstrom resolution. *Science* **1998**, *282*, 1853-1858.

3 Lemon, B. J.; Peters, J. W. Binding of Exogenously Added Carbon Monoxide at the Active Site of the Iron-Only Hydrogenase (CpI) from Clostridium pasteurianum. *Biochemistry* **1999**, *38*, 12969 -12973.

4 Nicolet, Y.; De Lacy, A. L.; Vernéde, X.; Fernandez, V. M.; Hatchikian, E. C.; Fontecilla-Camps, J. C. Crystallographic and FTIR Spectroscopic Evidence of Changes in Fe Coordination Upon Reduction of the Active Site of the Fe-Only Hydrogenase from Desulfovibrio desulfuricans. *J. Am. Chem. Soc.* **2001**, *123*, 1596-1601.

5 Lubitz, W.; Ogata, H.; Rűdiger, O.; Reijerse, E. Hydrogenases. *Chem. Rev*. **2014**, *114*, 4081-4148.

6 Sommer, C.; Adamska-Venkatesh, A.; Pawlak, K.; Birrell, J. A.; Rűdiger, O.; Reijerse, E. J.; Lubitz, W. Proton Coupled Electronic Rearrangement within the H-Cluster as an Essential Step in the Catalytic Cycle of [FeFe] Hydrogenases. *J. Am. Chem. Soc*. **2017**, *129*, 1440-1443.

7 Wittkamp, F.; Senger, M.; Stripp, S. T.; Apfel, U.-P. [FeFe]-Hydrogenases: recent developments and future perspectives. *Chem. Commun*. **2018**, *54*, 5934-5942.

8 Thoi, V. S.; Sun, Y.; Long, J. R.; Chang, C. J. Complexes of earth-abundant metals for catalytic electrochemical hydrogen generation under aqueous conditions. *Chem. Soc. Rev*. **2013**, *42*, 2388-2400.

9 Georgakaki, I. P.; Thomson, L. M.; Lyon, E. J.; Hall, M. B.; Darensbourg, M. Y. Fundamental properties of small molecule models of Fe-only hydrogenase: computations relative to the definition of an entatic state in the active site. *Coord. Chem. Rev.* **2003**, *238-239,* 255-266.

10 Evans, D. J.; Pickett, C. J. Chemistry and the hydrogenases. *Chem. Soc. Rev*. **2003**, *32*, 268-287.

View Article Online
DOI: 10.1039/D0DT00946H

11 Rauchfuss, T. B. Research on soluble metal sulfides: from polysulfido complexes to functional models for the hydrogenases. *Inorg. Chem*. **2004**, *43*, 14-26.

12 Sun, L.; Åkermark, B.; Ott, S. Iron hydrogenase active site mimics in supramolecular systems aiming for light-driven hydrogen production. *Coord. Chem. Rev*. **2005**, *249*, 1653-1663.

13 Liu, X.; Ibrahim, S. K.; Tard, C.; Pickett, C. J. Iron-only hydrogenase: Synthetic, structural and reactivity studies of model compounds. *Coord. Chem. Rev*. **2005**, *249*, 1641-1652.

14 Capon, J. -F.; Gloaguen, F.; Schollhammer, P.; Talarmin, J. Catalysis of the electrochemical H_2 evolution by di-iron sub-site models. *Coord. Chem. Rev*. **2005**, *249*, 1664-1676.

15 Capon, J. -F.; Gloaguen, F.; Pétillon, F. Y.; Schollhammer, P.; Talarmin, J. Organometallic diiron complex chemistry related to the $[2Fe]_H$ subsite of $[FeFe]H_2$ase. *Eur. J. Inorg. Chem*. **2008**, 4671-4681.

16 Tard, C.; Pickett, C. J. Structural and Functional Analogues of the Active Sites of the [Fe]-, [NiFe] and [FeFe]-Hydrogenases. *Chem. Rev*. **2009**, *109*, 2245-2274.

17 Simmons, T. R.; Berggren, G.; Bacchi, M.; Fontecave, M. V.; Artero, V. Mimicking hydrogenases: From biomimetics to artificial enzymes. *Coord. Chem*. *Rev*. **2014**, *270-271*, 127-150.

18 Schilter, D.; Camara, J. M.; Huynh, M. T.; Hammes-Schiffer, S.; Rauchfuss, T. B. Hydrogenase Enzymes and Their Synthetic Models: The Role of Metal Hydrides. *Chem. Rev*. **2016**, *116*, 8693-8749.

19 Arrigoni, F.; Bertini, L.; Breglia, R.; Greco, C.; De Gioia, L.; Zampella, G. Catalytic H2 evolution/oxidation in [FeFe]-hydrogenase biomimetics: account from DFT on the interplay of related issues and proposed solutions. *New J. Chem*. **2020**, *44*, 17596-17615.

20 Kleinhaus, J. T.; Wittkamp, F.; Yadav, S.; Siegmund, D.; Apfel. U. -P. [FeFe]-Hydrogenases: maturation and reactivity of enzymatic systems and overview of biomimetic models. *Chem. Soc. Rev*. **2021**, *50*, 1668-1784.

21 Liu, Y. -C. C.; Yen, T. -H. H.; Chu, K. -T. T.; Chiang, M.-H. Utilization of Non-Innocent Redox Ligands in [FeFe] Hydrogenase Modeling for Hydrogen Production. *Comments Inorg. Chem*. **2015**, *36*, 141–181.

22 Tard, C.; Liu, X.; Ibrahim, S. K.; Bruschi, M.; De Gioia, L.; Davies, S. C.; Yang, X.; Wang, L. -S.; Sawers, G.; Pickett, C. J. Synthesis of the H-cluster framework of iron-only hydrogenase. *Nature* **2005**, *433*, 610-613.

23 Qian, G.; Zhong, W.; Wei, Z.; Wang, H.; Xiao, Z.; Long, L.; Liu, X. Diiron hexacarbonyl complexes bearing naphthalene-1,8-dithiolate bridge moiety as mimics of the sub-unit of [FeFe]-hydrogenase: synthesis, characterisation and electrochemical investigations. *New J. Chem*. **2015**, *39*, 9752–9760.

24 Lansing, J. C.; Camara, J. M.; Gray, D. E.; Rauchfuss, T. B. Hydrogen Production Catalyzed by Bidirectional, Biomimetic Models of the [FeFe]-Hydrogenase Active Site. *Organometallics* **2014**, *33*, 5897-5906.

25 Si, Y.; Charreteur, K.; Capon, J. -F.; Gloaguen, F.; Pétillon, F. Y.; Schollhammer, P.; Talarmin, J. Non-innocent bma ligand in a dissymetrically disubstituted diiron dithiolate related to the active site of the [FeFe] hydrogenases. *J. Inorg. Biochem*. **2010**, *104*, 1038-1042.

26 Becker, R.; Amirjalayer, S.; Li, P.; Woutersen, S.; Reek, J. N. H. An iron-iron hydrogenase mimic with appended electron reservoir for efficient proton reduction in aqueous media. *Sci. Adv*. **2016**, *2*, e1501014.

27 Qian, G.; Wang, H.; Zhong, W.; Liu, X. Electrochemical investigation into the electron transfer mechanism of a diiron hexacarbonyl complex bearing a bridging naphthalene moiety. *Electrochim. Acta* **2015**, *163*, 190–195.

28 de Hatten, X.; Bothe, E.; Merz, K.; Huc, I.; Metzler-Nolte, N. A Ferrocene–Peptide Conjugate as a Hydrogenase Model System. *Eur. J. Inorg. Chem*. **2008**, 4530-4537.

29 Zeng, X.; Li, Z.; Xiao, Z.; Wang, Y.; Liu, X. Using pendant ferrocenyl group(s) as an intramolecular standard to probe the reduction of diiron hexacarbonyl model complexes for the sub-unit of [FeFe]-hydrogenase. *Electrochem. Commun*. **2010**, *12*, 342-345.

30 Zhao, J.; Wei, Z.; Zeng, X. Liu, X. Three diiron complexes bearing an aromatic ring as mimics of the diiron subunit of [FeFe]-hydrogenase: synthesis, electron transfer and coupled chemical reactions. *Dalton Trans*. **2012**, *41*, 11125-11133.

31 Arrigoni, F.; Bertini, L.; Bruschi, M.; Greco, C.; De Gioia, L. Zampella, G. H_2 Activation in [FeFe]-Hydrogenase Cofactor Versus Diiron Dithiolate Models: Factors Underlying the Catalytic Success of Nature and Implications for an Improved Biomimicry. *Chem. Eur. J.* **2019**, *25*, 1227–1241.

32 Camara, J. M.; Rauchfuss, T. B. Combining acid-base, redox and substrate binding functionalities to give a complete model for the [FeFe]-hydrogenase. *Nature Chem.* **2012**, *4*, 26-30.

33 Ghosh, S.; Hogarth, G.; Hollingsworth, N.; Holt, K. B.; Kabir, S. E.; Sanchez, B. E. Hydrogenase biomimetics: $Fe_2(CO)_4$(μ-dppf)(μ-pdt) (dppf = 1,1'-

bis(diphenylphosphino)ferrocene)) both a proton-reduction and hydrogen oxidation catalyst. *Chem. Commun*. **2014**, *50* 945–947.

34 Wang, N.; Wang, M.; Wang, Y.; Zheng, D.; Han, H.; Ahlquist, M. S. G.; Sun, L. Catalytic Activation of H_2 under Mild Conditions by an [FeFe]-Hydrogenase Model via an Active μ-Hydride Species. *J. Am. Chem. Soc*. **2013**, *135*, 13688-13691.

35 Orton, G. R. F.; Belazregue, S.; Cockcroft, J. K.; Hartl, F.; Hogarth, G. Biomimics of [FeFe]-hydrogenases: Synthesis, molecular structures and protonation-oxidation and redox chemistry of $[Fe_2(CO)_4\{\mu\text{-}S(CH_2)_nS\}\{\kappa^2\text{-}(Ph_2PCH_2)_2NR\}]$ (n = 2, 3; R = Me, Bn) as H_2 oxidation catalysts. *J. Organomet. Chem.* **2023**, *991*, 122673.

36 Simmons, T. R.; Artero, V. Catalytic Hydrogen Oxidation: Dawn of a New Iron Age. *Angew. Chem., Int. Ed*. **2013**, *52*, 6143-6145.

37 Ahmed, E. Md; Dey, S.; Darensbourg, M. Y. ; Dey, A. Oxygen-Tolerant H_2 Production by [FeFe]-H_2ase Active Site Mimics Aided by Second Sphere Proton Shuttle. *J. Am. Chem. Soc*. **2018**, *140*, 12457-12468.

38 Ahmed, E. Md ; Nayek, A.; Krizan, A.; Coutard, N.; Morozan, A.; Ghosh Dey, S.; Lomoth, R.; Hammarstrom, L.; Artero, V.; Dey, A. A bidirectional bioinspired [FeFe]-hydrogenase model. *J. Am. Chem. Soc.* **2022**, *144*, 3614-3625.

39 Ghosh, S.; Rahaman, A.; Hollingsworth, N.; Nordlander, E.; Holt, K. B.; Richmond, M. G.; Kabir, S. E.; Hogarth, G. Hydrogenase biomimetics with redox active ligands: Catalytic proton reduction by $[Fe_2(CO)_4(\kappa^2\text{-diamine})(\mu\text{-edt})]$ (diamine = 2,2'-bipy, 1,10-phen). *Polyhedron* **2016**, *116,* 127-135.

40 Ghosh, S.; Rana, S.; Hollingsworth, N.; Richmond, M. G.; Kabir, S. E.; Hogarth, G. Synthesis, structure and electrocatalytic studies on $Fe_2(CO)_4(\kappa^2\text{-dppn})(\mu\text{-edt})$ (edt = ethanedithiolate; dppn = 1,8-bis(diphenylphosphino)naphthalene). *Inorganics* **2018**, *6*, 122-136.

41 Ghosh, S.; Rana, S.; Kabir, S. E.; Richmond, M. G.; Hogarth, G. Highly efficient electrocatalytic proton-reduction by coordinatively and electronically unsaturated square-pyramidal $Fe(CO)(\kappa^2\text{-dppn})(\kappa^2\text{-tdt})$. *J. Organomet. Chem*. **2019**, *486*, 435-440.

42 Ghosh, S.; Hollingsworth, N.; Warren, M.; Hrovat, D. A.; Richmond, M. G.; Hogarth, G. Hydrogenase biomimics containing redox-active ligands: $Fe_2(CO)_4(\mu\text{-edt})(\kappa^2\text{-bpcd})$ with electron-acceptor 4,5-bis(diphenylphosphino)-4-cyclopenten-1,3-dione (bpcd) as a potential $[Fe_4\text{-}S_4]_H$ surrogate. *Dalton Trans*. **2019**, *48*, 6051-6060.

43 Orton, G. R. F.; Ghosh, S.; Alker, L.; Sarker, J. C.; Pugh, D.; Richmond, M. G.; Hartl, F.; Hogarth, G. Biomimics of [FeFe]-hydrogenases incorporating redox-active ligands: synthesis, redox properties and spectroelectrochemistry of diiron-dithiolate complexes with ferrocenyl-diphosphines as Fe_4S_4 surrogates. *Dalton Trans*. **2022**, *51*, 9748-9769.

44 Orton, G. R. F.; Pižl, M.; Belazregue, S.; Lake, A. J.; Elsegood, M. R. J.; Cockcroft, J. K.; Smith, M. B.; Hartl, F.; Hogarth, G. Oxidation path and protonation of $[Fe_2(CO)_4(\mu\text{-edt})\{\kappa^2\text{-}(R_2PCH_2)_2NCH_2Fc\}]$ (R = Ph, Cy) biomimetics of [FeFe]-hydrogenases incorporating a proton-relay and a second redox center. *Inorganics* **2026**, *14*, 83.

45 Orton, G. R. F.; Ringenberg, M. R.; Hogarth, G. Biomimetics of [FeFe]-hydrogenases incorporating redox-active ligands: Ferrocene-bridged dithiolate complexes $Fe_2(CO)_6(\mu\text{-}EC_5H_4FeC_5H_4)$ (E = S, Se). *J. Organomet. Chem*. **2022**, *978*, 122472

46 Häßner, M.; Fiedler, J.; Ringenberg, M. R. Spectroelectrochemical and Electrocatalytic Investigation of 1,1'-Dithiolatoferrocene-Hexacarbonyldiiron. *Inorg. Chem*. **2019**, *58*, 1742–1745.

47 Seyferth, D.; Hames, B. W. Synthesis of μ,μ'-(1,1'-dithiolatoferrocene) hexacarbonyldiiron. *Inorg. Chim. Acta* **1983**, *77*, L1-L2.

48 Mathur, P.; Raghuvanshi, A.; Mobin, S. M. Reactivity of 1,2,3-triselena[3]ferrocenophane towards transition metal carbonyls. *J. Organomet. Chem*. **2015**, *794*, 266–273.

49 Felton, G. A. N.; Mebi, C. A.; Petro, B. J.; Vannucci, A. K.; Evans, D. H.; Glass, R. S.; Lichtenberger, D. L. Review of electrochemical studies of complexes containing the Fe_2S_2 core characteristic of [FeFe]-hydrogenases including catalysis by these complexes of the reduction of acids to form dihydrogen. *J. Organomet. Chem*. **2009**, *694*, 2681-2699.

50 Hogarth, G. Unexpected leading roles for $[Fe_2(CO)_6(\mu\text{-pdt})]$ in our understanding of [FeFe]-H_2ases and the search for clean hydrogen production *Coord. Chem. Rev*. **2023**, *490*, 215174.

51 Gao, W.; Ekström, J.; Liu, J.; Chen, C.; Eriksson, L.; Weng, L.; Åkermark, B.; Sun, L. Binuclear Iron-Sulfur Complexes with Bidentate Phosphine Ligands as Active Site Models of Fe-Hydrogenase and Their Catalytic Proton Reduction. *Inorg. Chem*. **2007**, *46*, 1981-1991.

52 Justice, A. K.; Zampella, G.; De Gioia, L.; Rauchfuss, T. B.; van der Vlugt, J. I.; Wilson, S. R. Chelate control of diiron(I) dithiolates relevant to the [Fe-Fe]-hydrogenase active site. *Inorg. Chem*. **2007**, *46*, 1655-1664.

53 Hogarth, G.; Richards, I. Synthesis, crystal structure and protonation of the asymmetric iron-only hydrogenase model $[Fe_2(CO)_3(\mu\text{-pdt})\{\mu,\kappa^3\text{-}Ph_2PCH_2CH_2P(Ph)CH_2CH_2PPh_2\}]$ (pdt = $SCH_2CH_2CH_2S$). *Inorg. Chem. Commun*. **2007**, *10*, 66-70.

54 Ghosh, S.; Sanchez, B. E.; Richards, I.; Haque, M. N.; Holt, K. B.; Richmond, M. G.; Hogarth, G. Biomimetics of the iron-only hydrogenase enzyme: Identification of kinetically favoured apical-basal $[Fe_2(CO)_4(\mu\text{-H})\{\kappa^2\text{-}Ph_2PC(Me_2)PPh_2\}(\mu\text{-pdt})]^+$ as a proton-reduction catalyst. *J. Organomet. Chem*. **2016**, *812*, 247-258.

55 Ghosh, S.; Hogarth, G.; Hollingsworth, N.; Holt, K. B.; Richard, I.; Richmond, M. G.; Sanchez, B.; Unwin, D. Models of the iron-only hydrogenase: A comparison of chelate and bridge isomers of $Fe_2(CO)_4\{Ph_2PN(R)PPh_2\}(\mu\text{-pdt})$ as proton reduction catalysts. *Dalton Trans*. **2013**, *42*, 6775-6792.

56 Huo, F.; Hou, J.; Chen, G.; Guo, D.; Peng, X. [FeFe]-Hydrogenase Models: Overpotential Control for Electrocatalytic H2 Production by Tuning of the Ligand π-Acceptor Ability. *Eur. J. Inorg. Chem*. **2010**, 3942-3951.

57 Li, P.; Wang, M.; He, C.; Li, G.; Liu, X.; Chen, C.; Akermark, B.; Sun, L. Influence of tertiary phosphanes on the coordination configurations and electrochemical properties of iron hydrogenase model complexes: Crystal structures of $[(\mu\text{-}S_2C_3H_6)Fe_2(CO)_{6-n}L_n]$ (L = PMe_2Ph, n = 1, 2; PPh_3, $P(OEt)_3$, n = 1). *Eur. J. Inorg. Chem*. **2005**, 2506-2513.

58 Li, P.; Wang, M.; He, C.; Liu, X.; Jin, K.; Sun, L. Phosphane and Phosphite Unsymmetrically Disubstituted Diiron Complexes Related to the Fe-Only Hydrogenase Active Site. *Eur. J. Inorg. Chem*. **2007**, 3718-3727.

59 Mejia-Rodriguez, R.; Chong, D.; Reibenspies, J. H.; Soriaga, M. P.; Darensbourg, M. Y. The Hydrophilic Phosphatriazaadamantane Ligand in the Development of H_2 Production Electrocatalysts: Iron Hydrogenase Model Complexes. *J. Am. Chem. Soc*. **2004**, *126*, 12004-12014.

60 Adam, F. I.; Hogarth, G.; Kabir, S. E.; Richards, I. Models of the iron-only hydrogenase: Synthesis and protonation of bridge and chelate complexes $[Fe_2(CO)_4\{Ph_2P(CH_2)_nPPh_2\}(\mu\text{-pdt})]$ (n = 2-4) – evidence for a terminal hydride intermediate. *Comp. Rend. Chim*. **2008**, *11*, 890-905.

61 Gloaguen, F.; Morvan, D.; Capon, J.-F.; Schollhammer, P.; Talarmin, J. Electrochemical proton reduction at mild potentials by monosubstituted diiron organometallic complexes bearing a benzenedithiolate bridge. *J. Electroanal. Chem*. **2007**, *603*, 15-20.

62 Schwartz, L.; Singh, P. S.; Eriksson, L.; Lomoth, R.; Ott, S. Tuning the electronic properties of $Fe_2(\mu$-arenedithiolate$)(CO)_{6-n}(PMe_3)_n$ (n =0, 2) complexes related to the [Fe-Fe]-hydrogenase active site. *Comp. Rend. Chim*. **2008**, *11*, 875-889.

63 Vannucci, A. K.; Wang, S.; Nichol, G. S.; Lichtenberger, D. L.; Evans, D. H.; Glass, R. S. Electronic and geometric effects of phosphatriazaadamantane ligands on the catalytic activity of an [FeFe] hydrogenase inspired complex. *Dalton Trans*. **2010**, *39*, 3050-3056.

64 Streich, D.; Karnahl, M.; Astuti, Y.; Cady, C. W.; Hammarstroem, L.; Lomoth, R.; Ott, S. Comparing the Reactivity of Benzenedithiolate- versus Alkyldithiolate-Bridged $Fe_2(CO)_6$ Complexes with Competing Ligands. *Eur. J. Inorg. Chem*. **2011**, 1106-1111.

65 Quentel, F.; Passard, G.; Gloaguen, F. A Binuclear Iron-Thiolate Catalyst for Electrochemical Hydrogen Production in Aqueous Micellar Solution. *Chem. Eur. J.* **2012**, *18*, 13473-13479.

66 Pandey, I. K.; Mobin, S. M.; Deibel, N.; Sarkar, B.; Kaur-Ghumaan, S. Diiron Benzenedithiolate Complexes Relevant to the [FeFe] Hydrogenase Active Site. *Eur. J. Inorg. Chem.* **2015**, *2015*, 2875-2882.

67 Roy, S.; Laureanti, J. A.; Groy, T. L.; Jones, A. K. Synthesis and Electrocatalytic Activity of [FeFe]-Hydrogenase Model Complexes with Non-Innocent Chelating Nitrogen-Donor Ligands. *Eur. J. Inorg. Chem*. **2017**, *2017*, 2942-2950.

68 Ellgen, P. C.; Gerlach, J. N. Kinetics and mechanism of the substitution reactions of bis(mercaptotricarbonyliron) complexes. *Inorg. Chem*. **1973**, *12*, 2526–2532.

69 Darensbourg, M. Y.; Lyon, E. J.; Smee, J. The bio-organometallic chemistry of active site iron in hydrogenases. *J. Coord. Chem. Rev*. **2000**, *206-207*, 533-561.

70 Li, Y.; Rauchfuss, T. B. Synthesis of Diiron(I) Dithiolato Carbonyl Complexes. *Chem. Rev*. **2016**, *116*, 7043-7077.

71 Song, L. C.; Gao, W.; Feng, C. P.; Wang, D. F.; Hu, Q. M. *Organometallics* **2009**, *28*, 6121–6130.

72 Wang, N.; Wang, M.; Liu, J.; Jin, K.; Chen, L.; Sun, L. *Inorg. Chem*. **2009**, *48*, 11551–11558.

73 Tye, J. W.; Darensbourg, M. Y.; Hall, M. B. De Novo Design of Synthetic Di-Iron(I) Complexes as Structural Models of the Reduced Form of Iron-Iron Hydrogenase. *Inorg.*

View Article Online
DOI: 10.1039/D6DT00946H

Chem. **2006**, *45*, 1552–1559.

74 Justice, A. K.; De Gioia, L.; Nilges, M. J.; Rauchfuss, T. B.; Wilson, S. R.; Zampella, G. Redox and structural properties of mixed-valence models for the active site of the [FeFe]-hydrogenase: progress and challenges. *Inorg. Chem*. **2008**, *47*, 7405–7414.

75 Adam, F. I.; Hogarth, G.; Richards, I. Models of the iron-only hydrogenase: Reactions of $[Fe_2(CO)_6(\mu\text{-pdt})]$ with small bite-angle diphosphines yielding bridge and chelate diphosphine complexes $[Fe_2(CO)_4(\text{diphosphine})(\mu\text{-pdt})]$. *J. Organomet. Chem*. **2007**, *692*, 3957-3968.

76 Barton, B. E.; Zampella, G.; Justice, A. K.; De Gioia, L.; Rauchfuss, T. B.; Wilson, S. R. Isomerization of the hydride complexes $[HFe_2(SR)_2(PR_3)_x(CO)_{6-x}]^+$ (x = 2, 3, 4) relevant to the active site models for the [FeFe]-hydrogenases. *Dalton Trans*. **2010**, *39*, 3011-3019.

77 Wang, W.; Rauchfuss, T. B.; Zhu, L.; Zampella, G. New Reactions of Terminal Hydrides on a Diiron Dithiolate. *J. Am. Chem. Soc*. **2014**, *136*, 5773-5782.

78 Zaffaroni, R.; Rauchfuss, T. B.; Fuller, A.; De Gioia, L.; Zampella, G. Contrasting Protonation Behavior of Diphosphido vs Dithiolato Diiron(I) Carbonyl Complexes. *Organometallics* **2013**, *32*, 232-238.

79 Lu, X. L.; Ng, S. Y.; Vittal, J. J.; Tan, G. K.; Goh, L. Y.; Hor, T. S. A. Structural dynamics and ligand mobility in carboxylate and dithiocarbamate complexes of Ru(II) containing 1,1'-bis(diphenylphosphino)ferrocene (dppf). *J. Organomet. Chem*. **2003**, *688*, 100-111.

80 Cauzzi, D.; Graiff, C.; Massera, C.; Predieri, G.; Tiripiccho, A.; Acquotti, D. Chelating *versus* bridging behaviour and NMR fluxionality of dppf in the *nido* clusters $[M_3Se_2(CO)_7(\text{dppf})]$ [M = Fe or Ru, dppf = $Fe(\eta^5\text{-}C_5H_4PPh_2)_2$]. Crystal structure of the chelated ruthenium derivative. *J. Chem. Soc., Dalton Trans*. **1999**, 3515-3521.

81 Bandoli, G.; Dolmella, A. *Coord. Chem. Rev*. **2000**, *209*, 161-196. (d) Young, D. J.; Chien, S. W.; Hor, T. S. A. 1,1'-Bis(diphenylphosphino)ferrocene in functional molecular materials. *Dalton Trans*. **2012**, *41*, 12655-12665.

82 Hogarth, G.; Kabir, S. E.; Richards, I. Diphosphine mobility at a binuclear metal centre: The concerted double trigonal-twist in bis(dithiolate) complexes $[M_2(CO)_4(\mu\text{-dppm})\{\mu\text{-}S(CH_2)_nS\}]$ (M = Fe, Ru; *n* = 2, 3). *Organometallics* **2010**, *29*, 6559–6568.

83 Kunimatsu, K.; Seki, H.; Golden, W. G.; Gordon, J. G.; Philpott, M. R. *Langmuir* **1986**, *2*, 464–468.

84 de Menorval, L. -C.; Chaqroune, A.; Coq, B.; Figueras, F. *J. Chem. Soc. Faraday Trans.* **1997**, *93*, 3715–3720.

85 Zheng, D.; Wang, M.; Wang, N.; Cheng, M.; Sun, L. Effect of Bridgehead Steric Bulk on the Intramolecular C-H Heterolysis of [FeFe]-Hydrogenase Active Site Models Containing a P_2N_2 Pendant Amine Ligand. *Inorg. Chem*. **2016**, *55*, 411-418.

86 Georgakaki, I. P.; Miller, M. L.; Darensbourg, M. Y. Requirements for Functional Models of the Iron Hydrogenase Active Site: D_2/H_2O Exchange Activity in {(μ-SMe)(μ-pdt)$[Fe(CO)_2(PMe_3)]_2^+$}$[BF_4^-]$. *Inorg. Chem*. **2003**, *42*, 2489-2494.

87 Olsen, M. T.; Gray, D. L.; Rauchfuss, T. B.; De Gioia, L.; Zampella, G. Stereochemistry of electrophilic attack at 34e- dimetallic complexes: the case of diiron dithiolato carbonyls $MeS^{+\cdot}$ *Chem. Commun*. **2011**, *47*, 6554-6556.

88 Olsen, M. T.; Rauchfuss, T. B.; Zaffaroni, R. Reaction of Aryl Diazonium Salts and Diiron(I) Dithiolato Carbonyls: Evidence for Radical Intermediates. *Organometallics* 31 (2012) 3447-3450.

89 Liu, T.; Darensbourg, M. Y. A Mixed-Valent, Fe(II)Fe(I), Diiron Complex Reproduces the Unique Rotated State of the [FeFe]Hydrogenase Active Site. *J. Am. Chem. Soc*. **2007**, *129*, 7008-7009.

90 Justice, A. K.; Rauchfuss, T. B.; Wilson, S. R. Unsaturated, mixed-valence diiron dithiolate model for the H_{ox} state of the [FeFe] hydrogenase. *Angew. Chem., Int. Ed*. **2007**, *46*, 6152-6154.

91 Singleton, M. L.; Bhuvanesh, N.; Reibenspies, J. H.; Darensbourg, M. Y. Synthetic support of de novo design: sterically bulky [FeFe]-hydrogenase models. *Angew. Chem., Int. Ed.* **2008**, *47*, 9492-9495.

92 Hsieh, C.-H.; Erdem, O. F.; Harman, S. D.; Singleton, M. L.; Reijerse, E.; Lubitz, W.; Popescu, C. V.; Reibenspies, J. H.; Brothers, S. M.; Hall, M. B.; Darensbourg, M. Y. Structural and Spectroscopic Features of Mixed Valent $Fe^{II}Fe^{I}$ Complexes and Factors Related to the Rotated Configuration of Diiron Hydrogenase. *J. Am. Chem. Soc.* **2012**, *134*, 13089-13102.

93 Li, B.; Liu, T.; Singleton, M. L.; Darensbourg, M. Y. Influence of Sulf-Oxygenation on CO/L Substitution and $Fe(CO)_3$ Rotation in Thiolate-Bridged Diiron Complexes. *Inorg. Chem*. **2009**, *48*, 8393–8403.

94 Basato, M. Reaction of di-μ-(phenylthio)bis(tricarbonyliron) (Fe–Fe) with triphenylphosphine. Detailed kinetic and mechanistic study. *J. Chem. Soc., Dalton Trans.* **1975**, 911-917.

95 Krejčík, M.; Daněk, M.; Hartl, F. Simple construction of an infrared optically transparent thin-layer electrochemical cell. Applications to the redox reactions of ferrocene, decacarbonyldimanganese and (3,5-di-tert-butylcatacholato) tricarbonylmanganese(1-). *J. Electroanal. Chem. Interfacial Electrochem*. **1991**, *317*, 179-187.

96 Neese, F. The ORCA program system. *WIREs Comput. Mol. Sci.* **2012***, 2,* 73–78.

97 Becke, A D. Density-functional thermochemistry. III. The role of exact exchange. *J. Chem. Phys.* **1993**, *98*, 5648–5652.

98 Sheldrick, G. M. A short history of SHELX. *Acta Crystallogr., Sect. A* **2008**, *64*, 112-122.

99 Sheldrick, G. M. Crystal structure refinement with SHELXL. *Acta Crystallogr. C: Struct. Chem.* **2015**, *71*, 3-8.

100 McArdle, P. *Oscail*, a program package for small-molecule single-crystal crystallography with crystal morphology prediction and molecular modelling. *J. Appl. Crystallogr.* **2017**, *50*, 320-326.

101 Dolomanov, O. V.; Bourhis, L. J.; Gildea, R. J.; Howard, J. A. K.; Puschmann, H. OLEX2: a complete structure solution, refinement and analysis program. *J. Appl. Crystallogr.* **2009**, *42*, 339-341.

View Article Online
DOI: 10.1039/D6DT00946H

Data availability statement

The data that support the findings of this study are available on request from the corresponding author, [GH].